UNCONVENTIONAL PROTEIN SECRETION OF KERATIN 75 BY AMELOBLASTS *IN VIVO*

by

Xu Yang

Bachelor of Dental Medicine, Wuhan University, 2010

Master of Dental Medicine, Wuhan University, 2012

Submitted to the Graduate Faculty of

Dental Medicine School in partial fulfillment

of the requirements for the degree of

Doctor of Philosophy

University of Pittsburgh

2018

UNIVERSITY OF PITTSBURGH

School of Dental Medicine

This dissertation was presented

by

Xu Yang

It will be defended on

January 18, 2018

and approved by

Mark P Mooney, Professor, Dept of Oral Biology, U of Pittsburgh

Donna B Stolz, Associate Professor, Dept of Cell Biology, U of Pittsburgh

Heather L Szabo-Rogers, Assistant Professor, Dept of Oral Biology, U of Pittsburgh

Dissertation Advisor: Elia Beniash, Professor, Dept of Oral Biology, U of Pittsburgh

Unconventional Protein Secretion of Keratin 75 by Ameloblasts *in vivo*

Xu Yang, DDS/Master

University of Pittsburgh, 2018

Keratin-75, originally identified as a hair follicle specific keratin, was recently discovered in enamel tissue. Individuals carrying a K75 A161T mutation presented with altered enamel structure and increased susceptibility to dental caries. The first objective of this dissertation is to verify the existence of K75 in enamel tissue and to study its distribution, especially the subcellular localization in ameloblasts. We confirmed the existence the K75 in ameloblasts, stratum intermediate and enamel matrix through in situ hybridization, immunofluorescence(IF), and mass spectrometry. K75 expression in forming rodent teeth was confined to the secretory stage ameloblasts in IF studies. Unlike other cytokeratins, such as K14, which forms fibrillar networks, K75 was found in large granular bodies and diffuse signal in ameloblast cell body and Tomes' processes. Consistent with IF observations, immuno-gold transmission electron microscopy(IG-TEM) studies detected K75 in large and small membrane-delineated vesicles located in ameloblast cell body and Tomes' processes. Moreover, the majority of K75 signal overlapped with enamel matrix proteins(EMPs) ameloblastin and amelogenin in both types of vesicles.

IF and IG-TEM data strongly indicate that K75, traditionally regarded as a component of cytoskeleton, is secreted by ameloblasts together with other EMPs. Since K75 does not have a signal peptide, how K75 is transported out of the cell is intriguing. The second objective of this dissertation is to obtain insights into the trafficking pathway of K75. To address this objective, co-localization studies of K75 with organelle markers and conventional trafficking inhibition experiments were done. Under physiological conditions, K75 showed limited overlap with ER and lysosome markers, however it was highly co-localized with ER-Golgi-Intermediate-Compartment(ERGIC) and Golgi markers. When ER-Golgi trafficking was inhibited, ameloblastin was detained in rER lumen and isolated from Golgi apparatus whereas K75 still managed to translocate into the Golgi.

In summary, we demonstrate that localization of K75 in ameloblasts is different from typical cytokeratins. It is secreted extracellularly with EMPs by secretory stage ameloblasts. Moreover, our results suggest that K75 utilizes a novel unconventional protein secretion pathway which involves ERGIC and Golgi. This is the first time a secretory pathway for a cytosolic cytokeratin, lacking signaling peptide, was revealed.

TABLE OF CONTENTS

LIST OF FIGURES

PREFACE

I had laughter, I had joy, I had all the seasons in the sun,

I had tears, I had sorrow, I had all the nights in the moon.

I had a group of huckleberry friends sharing one the best time in my life,

I had a painful maturation making me realize who I am.

May the past belong to the past,

I still have the future in my hand.

1.0 INTRODUCTION

1.1 GENERAL

Enamel is the hardest tissue in mammals, and mature enamel comprises 95% carbonated hydroxyapatite mineral and approximately 1% organic matrix. Enamel formation (amelogenesis) is carried out by specialized epithelial cells, ameloblasts, in a highly coordinated multistep process. Enamel matrix deposition begins at the surface of forming dentin by presecretory ameloblasts. They differentiate into secretory ameloblasts, which are polarized cells with their nuclei located at the basal (proximal) pole and the Tomes' processes, specialized cellular secretory apparatus responsible for the enamel rod formation, at the apical (distal) pole (Figure 1). The majority of enamel matrix proteins (EMPs), of which amelogenin (AMELX) and ameloblastin (AMBN) account for more than 90%, are secreted extracellularly by ameloblasts at the secretory stage[1]. Rods and interrods are characteristic structures of enamel. The rod is a bundle of aligned crystals running wavily through the whole thickness of enamel, whereas interrod is a structure located in spaces between the rods, in which crystals are oriented differently from those of rods. They are formed in the secretary stage due to the unique morphology of Tomes' process[2-4]. Rods are woven into a very complex 3D structure, which is responsible for the unique mechanical resilience of this material[5-8]. Once the full thickness of enamel is deposited, the maturation stage begins, during which the majority of EMPs are

degraded and recycled. It is accompanied by active ion transportation and most importantly prominent hydroxyapatite crystallization. During enamel formation, mineral content rises from 30%(w/w) in the secretory stage to over 95%(w/w) in the mature form. Only a small fraction of a heavily crosslinked fibrous material remains in the mature enamel[9]. This material comprises rod sheaths, enveloping enamel rods, and enamel tufts, protein rich structures in the inner enamel[10,11].

Secretory stage amleloblasts are polarized cells with extensive ER and Golgi networks throughout the cell body. A scheme of ameloblast ultrastructure early ultrastructural studies[3,4,12-15], is shown in Fig. 1. A large cylindrical Golgi complex aligned with the long axis exists in the central portion of ameloblast[2,4]. The *cis* face of this central Golgi complex is mainly oriented towards the plasma membrane and the *trans* face towards the core of the cell, rich in vesicles. The space between the *cis* Golgi and plasma membrane is lined with the ER network. The very distal end of the ameloblast cell body, bordering the Tomes' process, is free of Golgi and rich in ER and secretory vesicles[4]. Small secretory/recycle vesicles are also full of Tomes process.

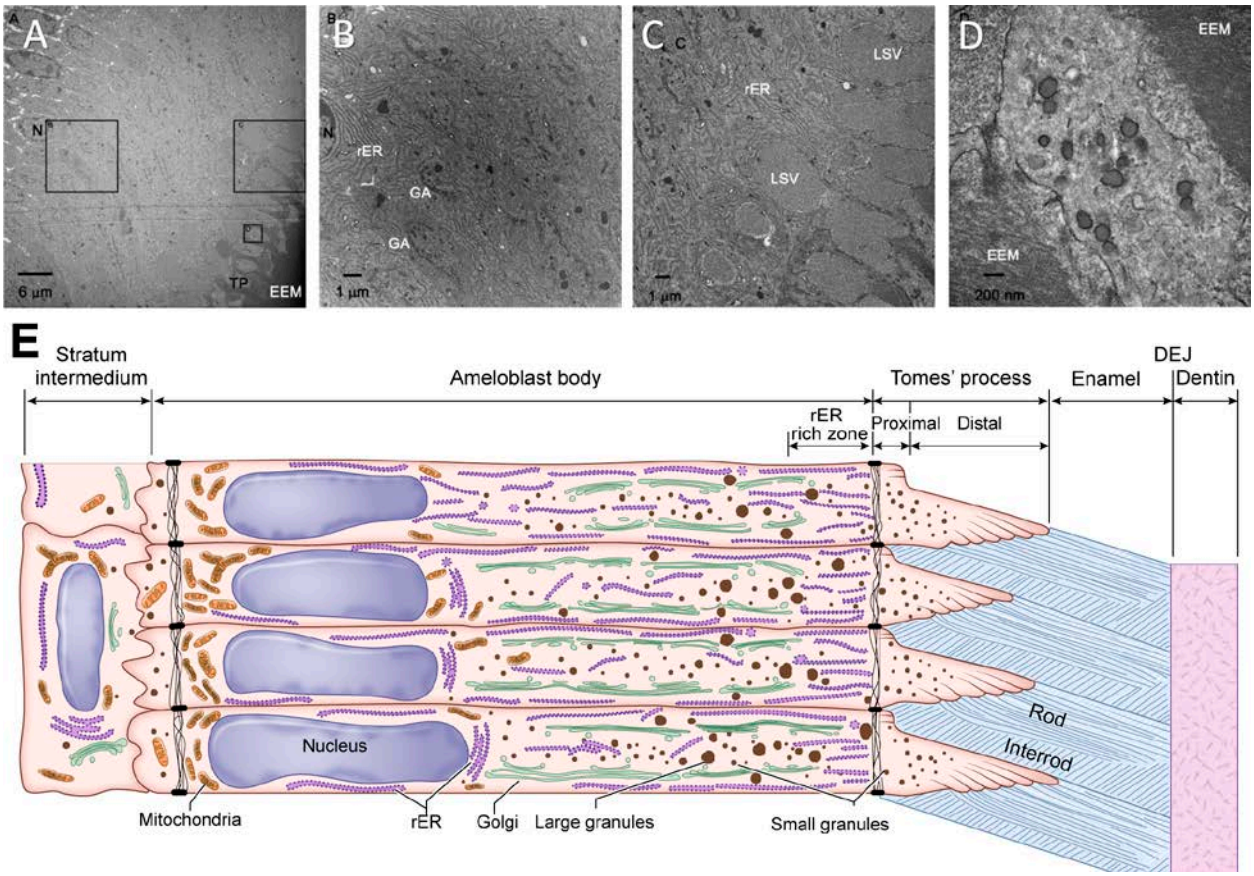

Figure 1. Ultra-structure of secretory stage ameloblasts.

(A-D) Ultra-structure of secretory stage ameloblasts under routine TEM. Boxes in panel A were magnified in panel B-D. (E) A scheme of secretary stage ameloblasts. N- nucleus; Tp-Tomes' process; EEM-extracellular enamel matrix; rER- rough endoplasmic reticulum; GA- Golgi apparatus; LSV- large secretory compartment.

1.2 INSOLUBLE PART OF ENAMEL

Organic matrix proteins play crucial roles in building up the hierarchical mineral structure of enamel[16]. Early researchers conducted several biochemical studies of the organics in forming mature teeth. They identified a fraction of the enamel matrix that is insoluble in both EDTA and hydrochloric acid[17-21]. This insoluble fraction was thought to form enamel tufts[22,23],

histologically recognizable structures protruding from dentin-enamel junction (DEJ) into enamel matrix, like tufts of grass. It was hypothesized that the tuft proteins exists at the beginning of enamel secretion and are highly cross-linked[10] and related to keratins[24,25] based on the amino acid composition of the mature enamel matrix[26], its high insolubility and the fact that enamel forming cells, ameloblasts, are of epithelial origin. In 1989, rabbit antisera against tuft extract was shown to react with some multivesicular structures in stratum granulosum layer of the rat foot pad, hinting toward a possibility that keratins might be present in enamel[24]. In 2011, Robinson et al.[10] showed by using antibodies to γ-glutamyl cross-linking peptide that tuft residues were heavily cross-linked via isopeptide bonds. However, due to the small quantities of EMPs in the tissue and their insolubility, the presence of keratins in enamel was never clearly established until recent discovery of keratin 75 (K75) in mature enamel[26].

1.3 K75 AND TEETH

Among 54 keratins currently identified in humans, about half are restricted to various compartments in hair follicles[27]. K75 is a type Ⅱ hair follicle-specific epithelial keratin. Winter et al.[28] first described its expression in the companion layer of anagen follicles. It was previously named K6hf because of its co-migration with K6 in gel and its specific expression pattern associated with hair follicles[28]. Later, studies revealed it also existed in the upper matrix and medulla of anagen hair follicle, secondary hair germ, non-cornified cells surrounding the cornified club of the telogen hair, nail bed epithelium and fungiform papillae of tongue[29,30]. Although some authors believe it belongs to K6 family, K75 shares the highest homology with K5 in its primary structure[31]. To date, at least three K75 genetic variants were studied. Chen et

al.[32] introduced a deletion of the highly conserved asparagine residue (N159) of K75 in mice. This deletion mimics the mutation of human K6A(N172), which leads to pachyonychia congenita. The affected mice showed impaired keratin cytoskeleton, abnormal anagen hair follicles, prominent hair shaft rupture and hypertrophic nails[32]. Lin et al.[33] described a K75 mutation in chicken with frizzle feather phenotype. The mutation is a deletion at exon 5 and intron 5 junction area, which caused cryptic splicing in exon 5, resulting in deletion of amino aicd 311-333. Winter et al.[34] reported a single-nucleotide polymorphism (SNP) of A161T that is associated with pseudofolliculitis barbae (PFB). PFB is a common disorder characterized by inflammation induced by ingrowing of hair into the adjacent skin region after regular shaving. It was shown that 76% of the regularly shaving men who carry A161T SNP have developed PFB[35]. Carriers of this SNP have a risk factor 6.12 times higher than the normal group. Together with curly hair, this K75 SNP act synergistically to increase the risk of PFB[36].

In 2014, Duverger et al.[37] provided the first direct evidence that K75 might exist in ameloblasts and enamel matrix. Importantly, they found that A161T SNP was associated with high prevalence of caries in humans. The effect of this polymorphism is dose dependent with carriers of two mutated alleles having highest caries score, followed by heterozygotes; and individuals who did not have this SNP had the lowest caries score. Carriers of A161T SNP presented with a dose dependent decrease in the inner enamel hardness and structural organization of enamel rods, rod sheaths and tufts. Another prominent feature of teeth associated with this SNP are long and narrow channels running from enamel surface to the DEJ. Taken together, these findings indicate that K75 plays an important role in amelogenesis and in mature enamel. At the same time, it remains unclear how K75 ends up in enamel.

1.4 CONVENTIONAL AND UNCONVENTIONAL PROTEIN SECRETION

Conventional protein secretion pathway requires a hydrophobic signal peptide at a N-terminus, which is essential for the synthesized protein to be translocated into the rough endoplasmic reticulum (rER) lumen [38,39]. Transmembrane proteins are targeted ER membrane via the C-tail anchoring mechanism[40]. In rER, nascent proteins undergo folding, oligomerization and N-linked glycosylation and sorting before transferring out of ER through specific regions called ER exit sites (ERES). Secreted proteins are transported in COP Ⅱ coated vesicles which bud from ERES[41]. The budding process is guided by a synergetic activity of several cage protein complexes, such as Sec16/Sec12, Sar1, Sec23/Sec24 and Sec13/Sec31[42,43]. COP Ⅱ coated vesicles are then fused with ER-Golgi-Intermediate-compartment (ERGIC) and the Cis-Golgi network. After entering Golgi apparatus, proteins undergo further posttranslational modifications, such as glycosylation and phosphorylation, etc. In the meantime, proteins travels through mid and trans-Golgi stack and trans-Golgi network (TGN), where they exit Golgi apparatus in secretory vesicles[44]. Departing from TGN, clathrin coated vesicles either fuse with plasma membrane and release their contents, or they are merged with the lysosome for degradation or secretion.

During the past decade, a large number of proteins, both cytosolic and secretory, were found to travel to the plasma membrane and extracellular space without entering ER-Golgi pathway. This alternative trafficking is called unconventional protein secretion (UPS). According to Nickel[45] and Rabouille[46], three types of pathways are described for cytosolic (leaderless) proteins to travel across plasma membrane, and secretory proteins (with a signal peptide) use two categories of unconventional secretion.

Type Ⅰ UPS pathway for leaderless proteins involves a pore-mediated translocation mechanism. Typical examples of this type include translocation of FGF2 and HIV TAT. FGF2 and TAT are recruited by phosphatidylinositol 4,5-bisphosphate (PI(4,5)P2) which is located in the leaflet of plasma membrane, and pass through a lipid membrane pore created by oligomerization[47-50]. Type Ⅱ pathway involves ATP-binding (ABC) based secretion, however its mechanism is not fully understood[51,52]. Type Ⅲ is autophagosome/endosome-based secretion. A typical example of this UPS type is IL-1β secretion[53,54]. IL-1β precursor is translocated across the secretory lysosome membrane together with caspase-1, which activates IL-1β by cleavage of the precursor and mature IL-1β is secreted out of the cell.

For proteins with signal peptides, two categories of UPS include COPⅡ vesicle bypass and Golgi bypass. Hsp150, a soluble yeast glycoprotein, is a typical example of secretory protein bypassing COPⅡ vesicles[55]. It exits rER through a specific ER site (ERES in yeasts) that is different from typical ERES, which is mediated by COPⅡ vesicles associated with Sec13 and Sec24. The best described example of secretory protein bypassing Golgi is cystic fibrosis transmembrane conductance regulator (CFTR), which is a membrane protein regulating chloride channel function. CFTR is believed to reach the plasma membrane by direct transport from ER by COPⅡ vesicles[56]. The trafficking is not affected by syntaxin 5 absence, which is a critical component of ER-Golgi pathway in all eukaryotes[57-59]. Moreover, by inducing an unconventional Golgi reassembly stacking protein(GRASP)-dependent secretion pathway, the disease-causing mutated CFTR which has impaired exocytosis could regain its surface expression.

As of now, the UPS is found in both stress-induced and constitutive circumstances. Although travelling in an unusual way, many UPS proteins seem to utilize the existing molecules

in the conventional trafficking pathway for their secretion. Some well-established molecules involved in UPS are from GRASP family, which are Golgi resident proteins helping to maintain the cisternae stacking organization. GRASP55/GRASP65 are found to play important roles in IL-1β secretion through autophagosome[60] and mutated CFTR secretion bypassing Golgi[56]. It is still not fully understood the reasons why such UPS pathways exist in all eukaryotes organisms, however there are potential benefits in utilizing these pathways. For example, UPS can provide a faster route of protein secretion in response to stress, extracellular stimulus or inflammation[61]. It is also a backup mechanism for normal secretion function when certain impairment (like ER stress) occurs in conventional trafficking. As more and more examples have been discovered as UPS, "one is tempted to speculate that what is termed unconventional protein secretion may not be that unconventional after all"[62]. The reason why it is termed unconventional may be merely because ER-Golgi pathway drew our attention in the first place.

1.5 SPECIFIC AIMS

A recent discovery of K75 in enamel tissue is the first clear evidence of keratins being a part of the enamel organic matrix[37]. The fact that a single amino acid substitution in this protein affects structural and mechanical properties of enamel, and is associated with the higher caries risk suggest that it plays important roles in enamel formation and function. At the same time, the expression pattern and localization of K75 in enamel tissue is still unclear. Furthermore, how K75, as a cytosolic protein lacking signal peptide, gets secreted extracellularly becomes an even more interesting mystery to uncover. This dissertation focuses on these important research questions which will be addressed in flowing specific aims.

Aim 1. To identify the expression and distribution pattern of K75 in forming enamel organ.

It is hypothesized that K75 is expressed in ameloblasts at least in secretory stage of amelogenesis, and is associated with enamel tufts and rod sheaths in the enamel matrix. The experiments outlined below are designed to test this hypothesis.

1) To study K75 mRNA and protein expression by in situ hybridization (ISH) and immuno-staining in rodent incisors at histological and ultrastructural levels in constantly growing rodent incisors.
2) To corroborate the existence of K75 in the enamel matrix by western blot and mass spectrometry.

Aim 2. To gain insights into the trafficking pathway of K75.

Our IF and IG-TEM studies conducted in Aim 1 show K75 in vesicles of different sizes, and being secreted from ameloblasts into the enamel matrix. This is a paradoxical observation, since keratins are normally considered as components of cytoskeleton, forming intermediate filament networks in epithelial cells. Moreover, keratins lack a signal peptide to guide them into ER. The site at which K75 enters ER-Golgi secretory pathwaysecretory pathway and routes in which it travels are mysteries. Thus, the second part of this thesis study will focus on the trafficking of K75 in ameloblasts. It's hypothesized that K75 is transported out of cytoplasm through UPS. Co-localization of K75 with three trafficking markers will be studied. Also, an ER-Golgi trafficking inhibition experiment by Brefeldin A (BFA), Monesin and H-89 will be used to provide more insights regarding the K75 secretory pathway.

1) To conduct co-localization studies of K75 with the secretory pathway markers, and determine at which stage it enters the secretory pathway. Specifically, co-localization of K75 with ER marker, ERGIC marker, Golgi marker and lysosome marker will be assessed in this

aim.

2) It will also be assessed if K75 secretion is ER-Golgi dependent by applying BFA, Monesin and H-89, inhibitors of conventional trafficking.

2.0 MATERIALS AND METHODS

2.1 RODENT MANSIBLE SAMPLES PREPARATION

All procedures described were approved by the University of Pittsburgh IACUC. Four-week old Sprague Dawley rats (Charles River, MA) and 4-week old mice (C57BL/6J, Jackson Laboratory, ME) were euthanized with CO2. Mandibles were dissected out quickly and immediately submersed in large volume of 4% paraformaldehyde in 10mM PBS, for IF or TEM, or Karnovsky fixative (2% glutaraldehyde, 2% formaldehyde in 10mM PBS), for TEM at 4℃. After 24 hours of fixation at 4℃, samples were placed into the demineralization solution, containing 0.1 M EDTA (pH 7.2-7.4) for one to two weeks. The demineralization solution was changed every other day. In some IG-TEM experiments, animals were anesthetized with isoflurane and perfused through the left ventricle first with cold PBS for 30 seconds then with cold 4% paraformaldehyde in 0.1M phosphate buffer or cold 1% Glutaraldehyde in 0.1M phosphate buffer for 15-20 minutes. The mandibles were dissected and further fixed in the same fixative solution for another 8-12 hours at 4℃, followed by demineralization, as described.

For IF, whole demineralized jaws were dehydrated using Leica ASP 300S automatic processer (Leica Biosystems, Buffalo Grove, IL) and paraffin embedded according to a standard protocol.

For TEM studies, after demineralization, mandibular bone around the incisors was trimmed and the molars were removed. The distal fragments of the jaws containing apical portions of the incisors were further cross-sectioned into 1-1.5 mm thick pieces, processed and embedded in LR White or Embed 812 (cat# 14381 and 14120, EMS, Hatfield, PA) according to published protocols[63]. In brief, for Embed 812 processing, incisor pieces were post-fixed in 1% ferrocyanide reduced osmium tetroxide for one hour, washed in PBS, dehydrated in graded ethanol and infiltrated with propylene oxide. The samples were embedded in Embed-812 and cured at 65°C for 2 days. For LR White processing, some of the samples were post-fixed in osmium tetroxide while others were not. Incisor pieces were washed in PBS, dehydrated in graded ethanol, embedded in LR White and cured at 60°C for 1-2 days.

For ISH, one-day postnatal mice were euthanized with CO_2 and fixed with 4% paraformaldehyde in 10mM PBS for 24 hours and embedded in paraffin according to standard procedures.

For IF and ISH, the paraffin blocks were sectioned using a Leica RM 2225 microtome (Leica Biosystems, Buffalo, IL) into 8 or 10 µm thick sections using a stainless-steel microtome knife (Leica 818, Leica, Germany). The sections were mounted on 3-Triethoxysilylpropylamine (440140, Millipore-Sigma, MO) coated glass slides. For TEM the resin blocks were sectioned into 70 nm thick sections using Leica EM UC7 ultramicrotome (Leica Biosystems, Buffalo, IL) equipped with diamond knife (EMS, Hatfield, PA). The sections were mounted on carbon coated Ni grids (EMS, Hatfield, PA).

2.2 IN SITU HYBRIDIZATION

Digoxin (DIG) conjugated probes targeted at the sense and antisense strands of mouse *Krt75* partial cDNA (421 bp) corresponding to exon 9 including the c-terminal tail domain and part of the 3' noncoding region (1494 to 1996 bp of Ref Seq NM 133357.3) were kindly provided by Maria Morasso (NIAMS/NIH, Bethesda, MD).

The ISH was performed according to a published protocol[64,65]. In brief, 10μm thick sections were used for in situ hybridization. Sections underwent de-paraffinization, rehydration, post-fixation, digestion, pre-hybridization in the first day, then were blocked in 10% sheep serum for 2 hours, incubated with 1:2000 anti-DIG ALP Antibody in 1% sheep serum mixture overnight at 4℃ at the second day, washed and incubated in developing solution (#1681451, Boehringer) at the third day. The reaction was stopped by PBS washing when signals showed up, then mounted in toluene (#4112, Thermo fisher).

2.3 IMMUNOFLUORESCENCE

Eight-μm paraffin sections were used for IF studies[66]. After de-paraffinization, sections were incubated with trypsin for 5-30 min at 37℃ or heated in citrate buffer for 10min for antigen retrieval, followed by blocking with 10% serum from secondary antibody host animal for 1 hour. The sections were incubated with primary antibodies at 4℃ overnight, washed in TBS and incubated with secondary antibodies for 45 min at room temperature. After final washes in TBS sections were incubated with 1.5% Sudan Black B (199664, Sigma, MO) in 70% Ethanol to

eliminate autofluorescence and counter-stained with DAPI. Primary antibodies used include rabbit anti-amelogenin, 1:1000 (ABT260, Abcam, MA), rabbit anti-amelogenin pS16 (a kind gift from Henry Margolis, Forsyth Institute, Boston, MA), goat anti-ameloblastin, 1:100 (sc-33102, Santa Cruz, CA), rabbit anti-ameloblastin, 1:100 (sc-50534, Santa Cruz, CA), goat anti-enamelin, 1:100 (sc-33107, Santa Cruz, CA), monoclonal rabbit anti calreticulin peptide 1, 4μg/ml (CP1, CPTC-CALR-1-s, Developmental Studies Hybridoma Bank, IA), mouse anti-PDI, 1:100 (NB300-517, Novusbio, CO), rabbit anti-GOLGA5, 1:100 (NBP1-83352, Novusbio, CO), goat anti-clathrin, 1:50 (sc-6579, Santa Cruz, CA), rabbit anti-ERGIC53, 1:100 (sc-66880, Santa Cruz, CA), rat anti-LAMP1, 4μg/ml (1D4B-s, DSHB, IA), rat anti-LAMP2, 4μg/ml (GL2A7-s, DSHB, IA), rabbit anti-GM130, 1:100 (Ab-52649, Abcam, MA), rabbit anti-Keratin 5, 1:2000 (905501, Biolegend, MA), rabbit anti-Keratin 14, 1:1000 (905301, Biolegend, MA), guinea pig anti-Keratin 75, 1:100 (20R-2647, Fitzgerald, MA), guinea pig anti-Keratin 27, 1:100 (20R-2639, Fitzgerald, MA), guinea pig anti-Keratin 25, 1:100 (20R-2637, Fitzgerald, MA). Secondary antibodies used include AlexaFlour-555/Cy3/Cy5 conjugated donkey anti-guinea pig/goat/rabbit/mouse/rat IgG(H+L), 1:400 purchased from Jackson Immunoresearch, PA.

Co-localization was calculated based on the number of pixels in a confocal z-stack which contain two channels. The % overlap was calculated as a ratio of overlapping pixels to the total number of pixels in each channel. For background adjustment adjacent sections were treated with naïve sera (isotype control) and signal intensity from these sections was used to determine the background fluorescence. The co-localization analysis was conducted using a proprietary Nikon software NIS Elements (Nikon, Melville, NY). The quantitative co-localization analysis was conducted on sections from 3 animals. The data was analyzed using t-test assuming unequal variance in OriginPro 2015 software package (Origin Labs, Northampton, MA).

2.4 POST-EMBEDDING IG-TEM

Seventy nm LR White or Embed 812 sections were used. Primary antibodies were 10 times more concentrated compared with immunofluorescence assay. Secondary antibodies include 6 nm colloidal gold conjugated donkey anti-guinea pig IgG, 1:30 (706-195-148, Jackson Immunoresearch, PA), 12 nm colloidal gold conjugated donkey anti-rabbit IgG, 1:30 (711-205152, Jackson Immunoresearch, PA). Sections were counter-stained with 2% Uranyl acetate for 10min. Other regents include normal guinea pig serum (88R-1015, Fitzgerald, MA) and rabbit serum (011-000-001, Jackson Immunoresearch, PA) as iso-type control.

2.5 CONVEENTIONAL TRAFFICKING INHIBITION EXPERIMENTS

Stock solution of BFA was prepared by dissolving BFA powder (B-8500, LC Laboratories, MA) in in DMSO at 25mg/ml. Twenty microliter of BFA was further dissolved in either 250µl DMSO, 30% ethanol or PBS for intraperitoneal (I.P.) injection. Each 4 weeks-old mouse received 0.5mg BFA and was sacrificed after 1, 3 and 5 hours (DMSO) or 1, 2, 3 hours (ethanol) or 15min, 30min, 1 hour (PBS).

Stock solution of Monesin (MNS) was prepared by dissolving MNS powder (M5273, Sigma, MO) in pure ethanol at 10 mg/ml. Half milligram MNS was further dissolved in 250µl 30% ethanol for I.P. injection. Each 4 weeks-old mouse received 0.5mg MNS and was sacrificed after 1 hour.

H-89 powder (H-5239, LC Laboratories, MA) was dissolved in DMSO at 100mg/ml and was used as stock solution. Half or 5mg of H-89 was further dissolved in 250µl 30% ethanol for I.P. injection. Each 4 weeks-old mouse received 0.5 or 5mg H-89 and was sacrificed after 1 hour.

2.6 MASS SPECTROMETRY

For mass spectrometry, healthy third molars were collected from clinics the School of Dental Medicine, University of Pittsburgh. Molars were fixed in 4% paraformaldehyde (PFA) for 3 days, washed with PBS, then subjected to demineralization in 10% EDTA (pH 7.4) for at least 2 weeks. Enamel tufts were collected by clean tweezers, and kept in fresh EDTA solution for another day, then washed in deionized water 3 times. Tufts were lyophilized using FreeZone 4.5 (Labconco, MO), milled into powder and processed according to a published procedure[67]. Five mg sample was incubated overnight at 37℃ in 0.4 mL 2% SDS/0.1 M sodium phosphate/25 mM DTE. Iodacetamide was added to the final volume of 50 mM and sample was stirred for 30 minutes at room temperature. Soluble and in-soluble parts were separated by centrifugation. For the soluble part, add 2.5×(volume) 100% ethanol, mix and collect the precipitates, rinse the precipitate from twice with 67% ethanol. For insoluble part, wash with 67% ethanol for four times and rinse with 0.1 M ammonium bicarbonate three times. Proteins were digested at room temperature with reductively methylated bovine trypsin (1% by weight) in 0.1 M ammonium bicarbonate-10% acetonitrile-1 mM $CaCl_2$ for 1 day (Previous soluble part, Fraction Ⅰ) and 2 days (Previous insoluble part) (add 40 µg trypsin again for the second day). Centrifuge and collect the supernate (Fraction Ⅱ) and still undissolved part. Undissolved part underwent

endoproteinase digestion (10μg in 200μl 0.1 M ammonium bicarbonate) at 37 ℃ for 1 day. Samples were centrifuged and supernate (Fraction Ⅲ) were collected. Finally, samples were submitted for mass spectrometry.

2.7 STATISTICAL ANALYSIS

For AMBN, K75 and AMELX IF co-localization experiments, three rats were utilized. Each rat has two to three stacks (around 10-slices each) measured for the overlap rate. For AMBN, K75 and AMELX IG-TEM co-localization experiments, three rats were utilized. One hundred to three hundred vesicles were taken into analysis for each rat. For BFA inhibition experiments in ethanol solvent, three mice were included for each group. Two sample paired t-test (SPSS, IBM, IL) was utilized to analyze the overlap differences between vehicle control and BFA treatment group.

3.0 DISTRIBUTION OF K75 IN ENAMEL RELATED TISSUE

3.1 EXPRESSION OF K75 MESSNGER RNA IN MOUSE ENAMEL RELATED TISSUE

The expression pattern of *Krt75* mRNA in the mouse head on the day 18 of the embryonic development was highly specific. *Krt75* was only expressed in hair/whisker follicles, and dorsal lingual papilla, in agreement previous reports[28,29] (Fig. 2C,D). In un-erupted incisor and molar teeth *Krt75* mRNA signal was located in ameloblasts and adjacent stratum intermedium of enamel organ (Fig. 2A,B). Quite surprisingly, odontoblasts, which are ectoderm mesenchymal cells, also expressed *Krt75*.

3.2 DETECTION OF K75 IN DEVELOPING PIG ENAMEL BY WESTERN BLOT

Western blot assay demonstrated the presence of K75 in forming pig enamel matrix (Fig. 2E). Strong bands were detected at both secretory and maturation stages was detected at ~60 KDa. In addition 2 weaker high molecular weight bands were detected at ~100 and 120 KDa, potentially corresponding to complexes of K75 with other proteins. Importantly, the no low molecular weight degradation products were detected in the maturating enamel, suggesting that K75 does not undergo proteolytic degradation as other EMPs.

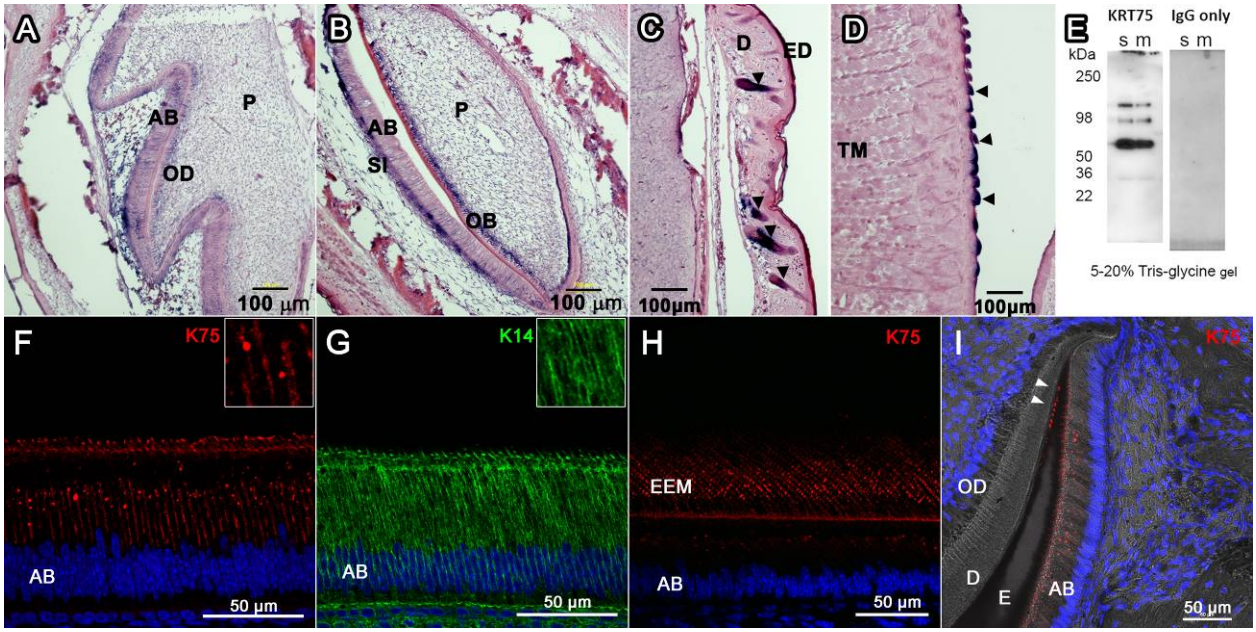

Figure 2. Localization of K75 in rodent and human teeth structure.

(A-D) ISH of *Krt75* in the craniofacial region of P1 mouse. (A, B) Expression of *Krt75* in the AB, SI and OD of P1 mouse molar and incisor. (C) *Krt75* is enriched in skin hair follicles. (D) *Krt75* is enriched in lingual papillae of P1 mouse tongue. (E) Western blot of un-erupted pig enamel matrix from secretory (s) and maturation (m) stages, K75 positive bands were detected around 60kDa. Two weaker bands at 100k and 120kDa were also observed. IgGs from naïve serum were used as an isotype control (F) K75 signal is present in mouse secretory ameloblasts as granules and diffuse band, diffuse signal is also detected in Tomes processes. (G) K14 signal is present in mice secretory ameloblasts in as tonofilament networks. K75 was also found in mouse EEM (H) and rat early forming enamel-dental junction (I, white triangles). P, pulp; OD, odontoblast; AB, ameloblast; D, dentin; E, enamel; SI, stratum intermedium; TM, tongue muscle; EEM, extracellular enamel matrix.

3.3 EXPRESSION OF K75 PROTEIN IN AMELOBLASTS AND FORMING ENAMEL

In order to determine when during tooth development K75 is expressed, IF study was conducted on constantly growing rodent incisors. Expression of two major enamel matrix proteins AMELX

and AMBN with known protein expression profiles were also assessed in the same sections. According to Katchburian and Holt [3], rat early ameloblast development could be divided into five regions (Fig. 3): Ⅰ, un-differentiation; Ⅱ, early differentiation; Ⅲ, intermediate differentiation; Ⅳ, late differentiation; Ⅴ, secretion without Tomes process; Ⅵ, secretion with Tomes process.

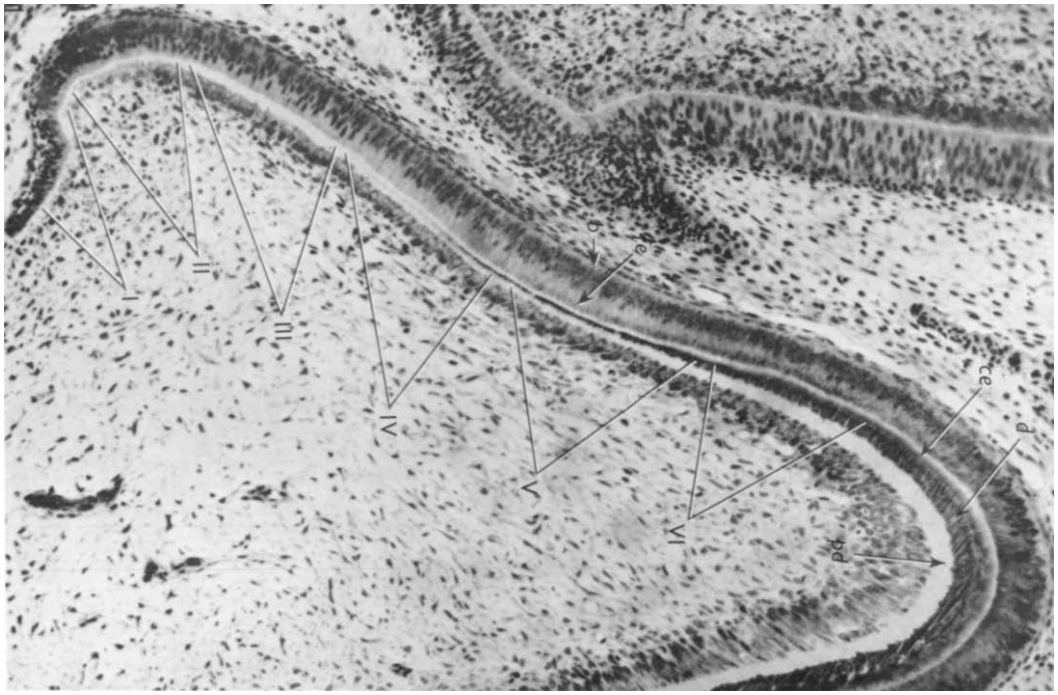

Figure 3. A section of cervical loop area from a 3-day-old rat's first molar.

The successive stages of differentiation of ameloblasts are indicated by regions I to VI: Region I undifferentiated ameloblasts, region II early differentiating ameloblasts, region III intermediate ameloblasts, region IV late differentiating ameloblasts, region V secretory ameloblasts without Tomes' process, region VI secretory ameloblasts with Tomes' process. Cited from Katchburian and Holt[3]. b, basal cytoplasm of ameloblasts; fe, distal cytoplasm of ameloblasts; ce, enamel; d, dentin; pd, predentin.

The onset of AMELX expression occurred as early as the intermediate to late differentiation stages, in both ameloblasts and opposing odontoblasts (Fig. 4B upper left,4C). Strong AMELX expression was observed in ameloblasts throughout the secretory stage and ceased at the

transition to maturation stage. A week AMBN signal appeared around region Ⅴ to Ⅵ, and continued throughout the secretory stage as well as the maturation stage (Fig. 4B lower). AMELX and AMBN protein expression profiles were consistent with literature reports[68-70]. Expression of K75 is mainly associated with the secretory stage ameloblasts. It began in region Ⅵ, shortly after the onset of AMBN and ceased at the maturation stage (Fig. 4B middle). In a typical actively secreting ameloblast, K75 was primarily located in the cell body of ameloblast and Tomes' process (Fig. 2F). A week signal of K75 was also observed in the stratum intermediate and occasionally in individual adjacent cells. K75 signal was present in either diffused form (potentially small aggregates) throughout the cell body and Tomes' processes and large granules. Large granules were located primarily in the distal half of the cell body. The appearance was radically different from that of typical cytokeratin K14, which formed dense networks of tonofilaments (Fig. 2G).

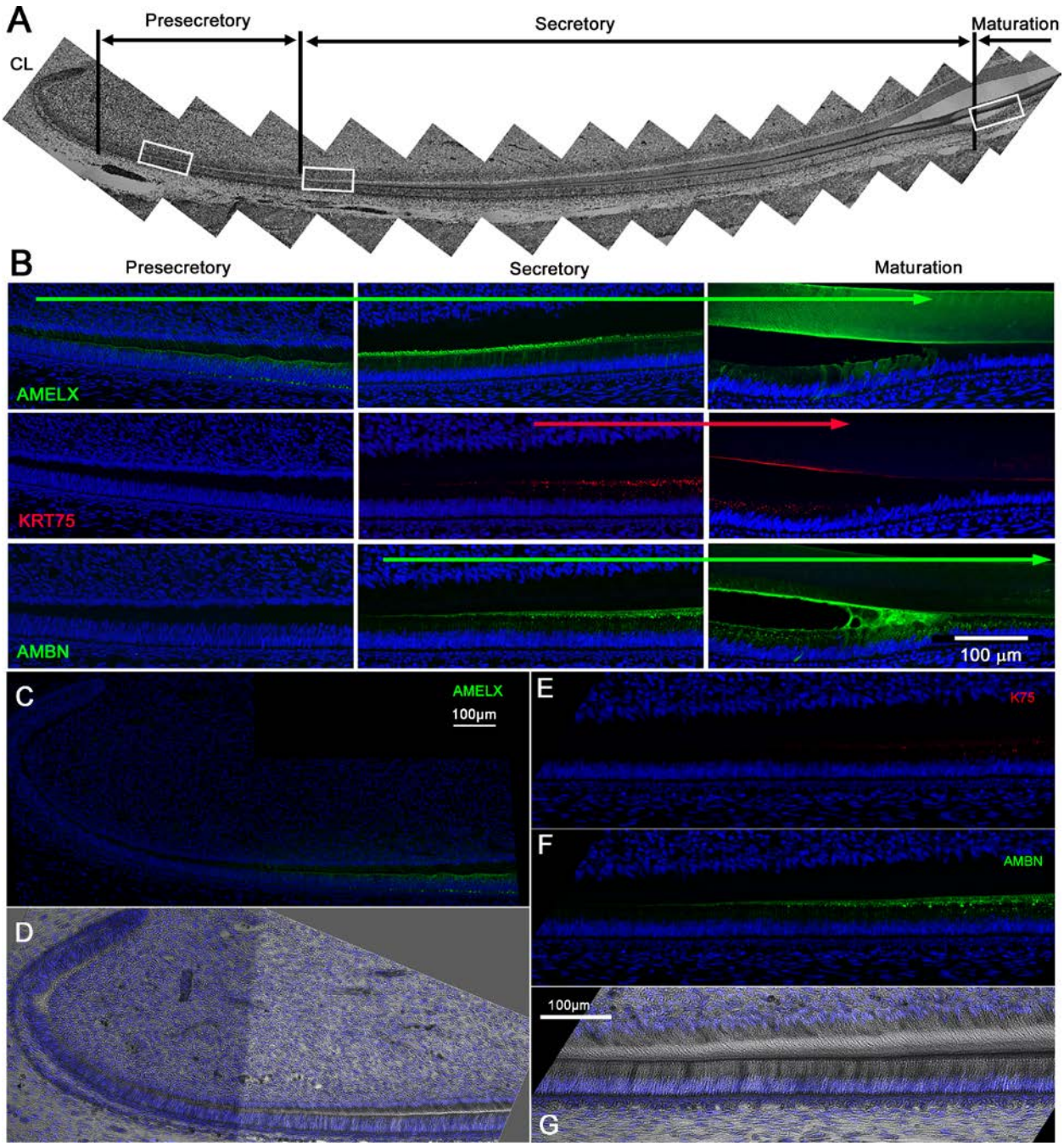

Figure 4. K75 expression in developing rat incisor.

(A) A bright field image of rat incisor section used in the IF study of AMELX, K75 and AMBN expression. Boxed areas are shown in panel B. (B) IF images of AMELX, K75 and AMBN in a continuously growing rat incisor. AMELX was found early in the presecretory stage ameloblasts and adjacent odontoblasts (upper row, left column) and its expression continued through the secretory stage and ceased at maturation stage (upper row, right column). Expression of K75 and AMBN started at secretory stage ameloblasts (mid column), and AMBN was detected a little

bit earlier than K75. Both proteins existed throughout the secretory stage. K75 expression ceased at maturation stage while AMBN expression continued through the maturation stage (right column). (C, D) Enlarged images of AMELX in pre-secretory stage ameloblasts. (E-G) Enlarged images of secretory stage ameloblast showing K75 and AMBN. CL, cervical loop.

K75 was also found in immature enamel matrix in the mouse samples. The signal appeared as chains of punctate following the direction of Tomes' process (Fig. 2H). Furthermore, in un-erupted third molars of rat, K75 signal appeared as discrete aggregates, resembling enamel tufts, at the early DEJ next to the cervical loop during the early secretory stage (Fig. 2I). However, these structures disappeared at the later stages of amelogenesis, possibly due to the heavy cross-linking.

Similar however more sophisticated results were obtained using IG-TEM. K75 was detected in ameloblasts, stratum intermedium and enamel matrix, but not in odontoblasts, dentin matrix, pulp tissue or periodontal ligament. In contrast to typical cytokeratin, no K75 was detected in association with tonofilaments of secretory ameloblasts. Instead, it was found in membrane delineated vesicles in the cell body and the Tomes' processes (Fig. 5). Based on the size and localization three groups of K75 positive vesicles were identified (Fig. 5A). First group contained small size vesicles (102.3±34.9 nm) located throughout the cell body from nucleus to distal junction complex (Fig. 5C). Second group consisted of similar size vesicles (88.7±20.2 nm) in Tomes' process (Fig. 5E). There were no significant differences in size between these two groups, however it is not clear whether they are the same population of vesicles. Middle to large size vesicles of irregular shapes (790.4±556.4 nm) in the distal half of cytoplasm comprised the third group (Fig. 5D)

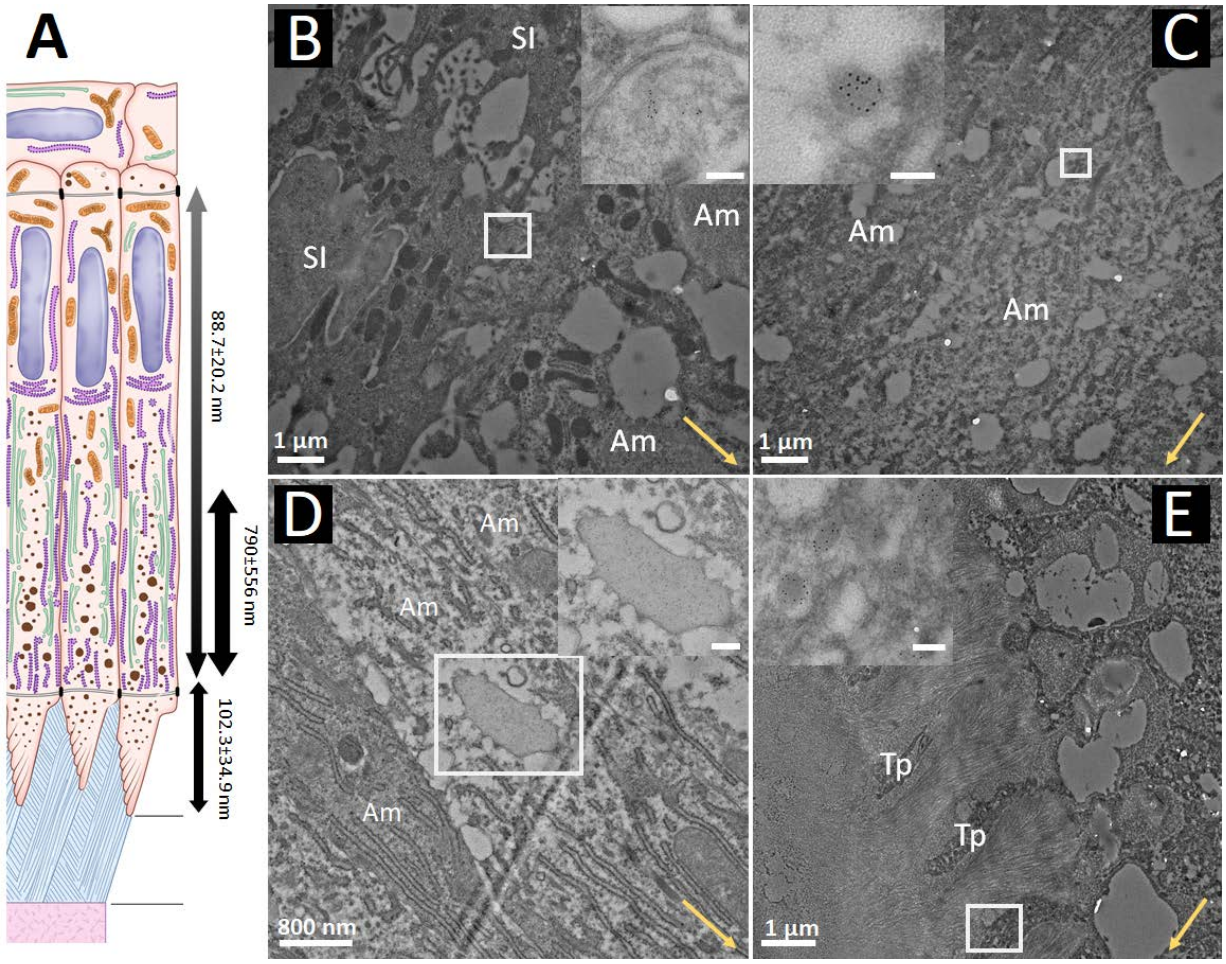

Figure 5. IG-TEM of K75 in rat incisor.

(A) Schematic image of secretory ameloblasts, the double-arrowed lines outline areas where K75 positive vesicles existed and the average diameter of the vesicles. (B) Small K75 positive vesicle around SI. (C) Small size K75 positive vesicle in distal cytoplasm. (D) Large size K75 positive vesicle located in distal cytoplasm. (E) Small size K75 positive vesicles in Tp. Yellow arrows point to the Tp along the long axis of ameloblast cell body. Scale bars in the insets are 100nm. Tp-Tomes' process; SI- stratum intermedium; Am- ameloblasts.

K75 also existed in the large secretory comportments (LSC) (4295.3±1280 nm), which existed in the distal end of ameloblast body and were proximal to Tomes' process, however at a much lower density (Fig. 6). All these results agreed with the results of the IF studies which also detected the larger granules in the distal portion of ameloblasts. The diffuse IF signal throughout the cell bodies and in the Tomes' processes can be attributed to the small vesicles identified

under TEM, which cannot be resolved by conventional light microscopy due to the diffraction limit.

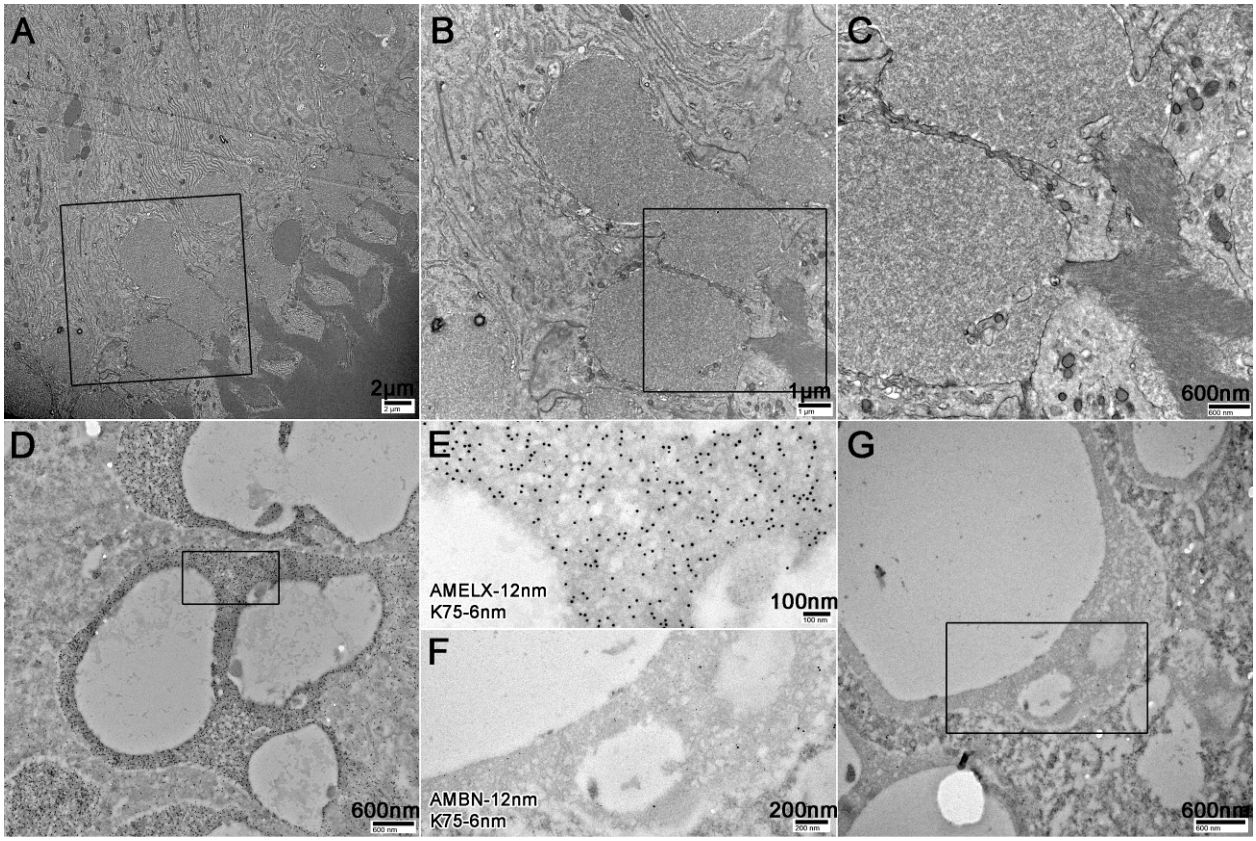

Figure 6. Large secretory compartments in rat ameloblasts.

(A-C) Ultra-structure of LSC in secretory ameloblasts. Black boxes in A and B were magnified in B and C. LSC was located in the distal end of ameloblast cell body, next to Tomes' process. The contents of some LSC are seen directly connected with EEM. (D, G) Co-labelling of AMELX&K75 and AMBN&K75 in LSC. Black boxes were further magnified in panel (E, F). LSC contain abundant of AMLEX and lower amounts of AMBN and K75.

3.4 MASS SPECTROMETRY OF HUMAN ENAMEL EXTRACTS

Human enamel tufts (Fig. 7A, B) are highly cross-linked that even after repeated SDS and enzymatic treatment there is still undissolved material. All dissolved fractions were subjected to

mass spectrometry analysis. In total, 423, 286, and 303 proteins were identified relatively in the fraction Ⅰ, Ⅱ, and Ⅲ, respectively (Fig. 7G). Some of the protein signatures, such as K1, K2, and K10 as well as albumin are likely contaminants while Col Ⅳ and laminin are remnants of the degraded basement membrane between pre-ameloblasts and pre-odontoblasts. The existence of Col Ⅺ was unexpected, because it usually appears in cartilage tissue[71]. Enamel matrix proteins, such as AMBN, ENAM, AMEL, MMP20, MMP14, KLK4, TIMPs[16], as well as mineralized tissue related proteins like DSPP, cadherin and calbindin are also identified by MS in the extracts. Several keratins such as K5, 6, 9, 14, 17, and 19 existed in all three fractions. Many keratin proteins have very similar sequences, thus making the grouping ambiguous. Although, the Mass spectrometry analysis of human tufts was not able identify K75 unequivocally, several sequences were identified which are shared between K75 and other hair follicle keratins, such as K5, K6A and K6C. Luckily, in the Mass Spectrometry of analysis of pig's enamel matrix, K75 specific sequence was able to be identified (Fig. 6H).

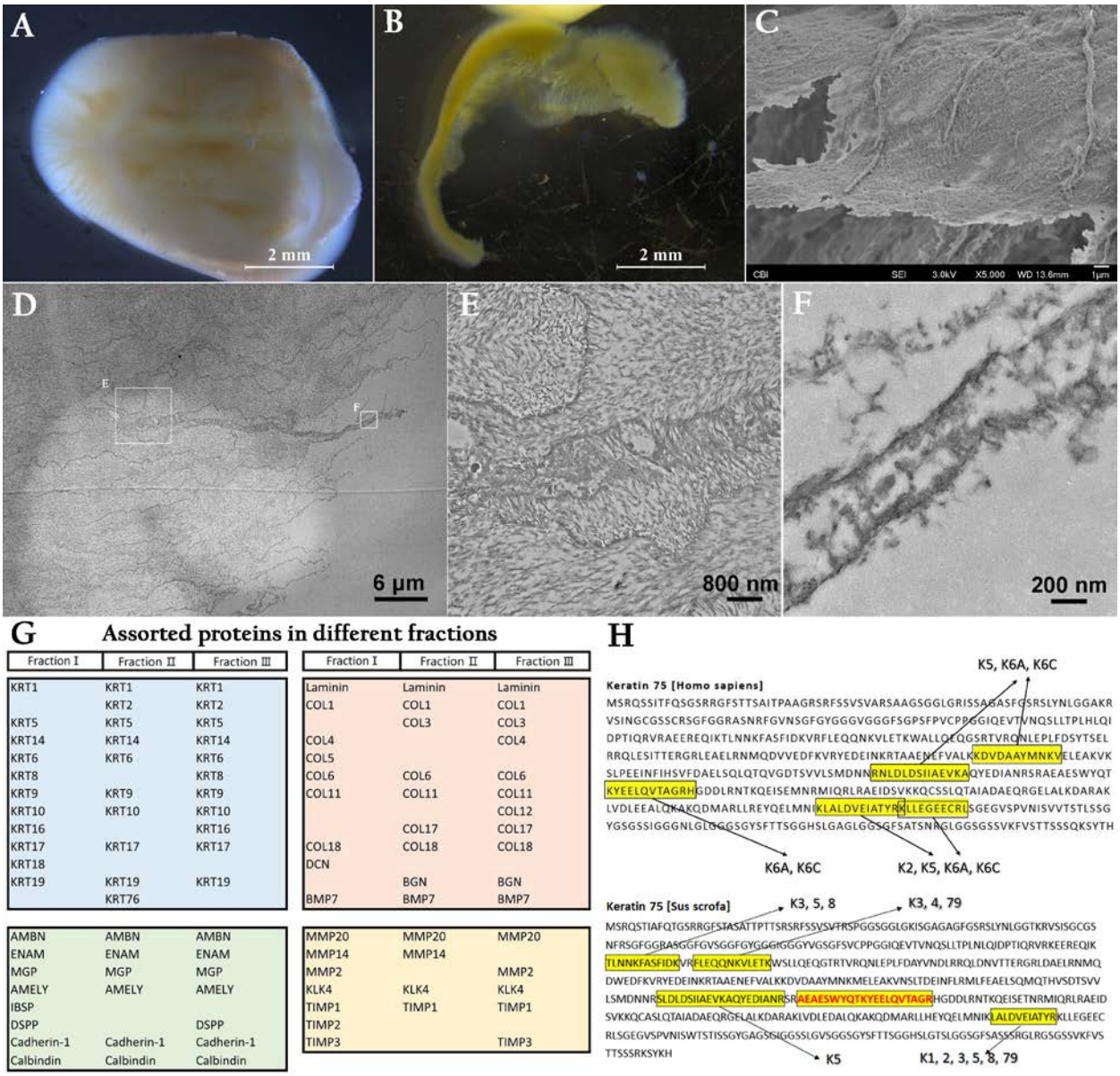

Figure 7. Human enamel tufts and mass spectrometry analysis.

(A) De-mineralized healthy human third molar crown, top view. Yellowish material covered on white dentin is the insoluble enamel matrix. (B) Insoluble enamel matrix peeled off from the crown. (C) A SEM micrograph of the insoluble organic fraction. Several large fibrils and multiple small fibrillar networks are apparent. (D-F) TEM micrographs of the insoluble enamel matrix. Panel D shows dense fibrillar networks of rod and rod sheath residues. White boxes are magnified in panel E and F. (G) Assorted proteins in different fractions of tufts. Proteins are grouped into four categories, shown in different colors. (H) K75 sequences detected in mass spectrometry are shown

in yellow frame. However, be noted they are overlapped with some other keratins. There is a K75 specific sequence shown in red font for pig enamel extractions.

3.5 CO-LOCALIZATION OF K75 AND EMPs

The intracellular localization pattern of K75, its presence in the membrane delineated compartments and in the extracellular space raise the possibility that it is secreted with the extracellular matrix proteins. To test this hypothesis, IF and IG TEM co-localization studies of K75 with two major EMPs, AMELX and AMBN were carried out.

In IF study, AMBN and AMELX showed considerable overlap with K75 throughout the cell body and the Tomes' processes, especially in the large vesicles, generally following the intracellular distribution pattern of K75 (Fig. 8). Triple labeling with K75, AMBN and AMELX antibodies revealed that in the ameloblast cell body, excluding the Tomes' process, ~80% and ~60% of K75 co-localized with AMBN and AMELX, ~50% of K75 co-localized with both AMBN and AMELX. Only ~10% of K75 did not overlap with AMBN nor AMELX. In contrast, more than 40% of AMBN and AMELX signal didn't overlap with other two proteins (Fig. 8K).

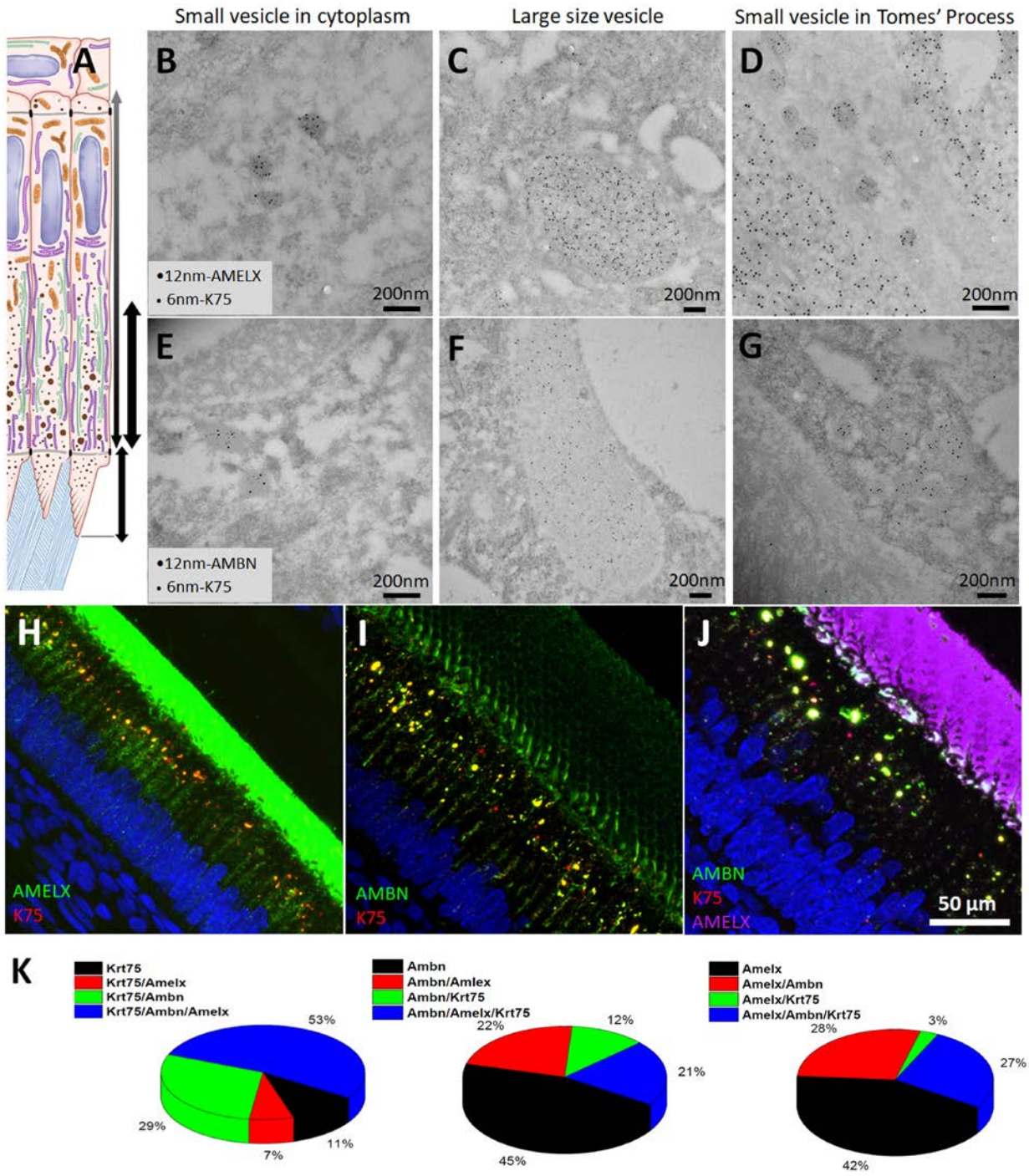

Figure 8. Co-localization of AMBN and AMELX with K75 in IG-TEM and IF.

(A) Schematic image of secretory ameloblasts. (B-D) IG-TEM co-localization of AMELX and K75 in the three groups of vesicles. (E-G) Co-localization of AMBN and K75 in the three groups of vesicles. (H-J) IF co-localization of AMELX, AMBN and K75 in secretory ameloblasts. (K) Pie chart showing the overlapping of K75 with AMELX

and AMBN based on the IF quantitative analysis of the incisal secretory amelobast cell bodies from 4-week-old rats (n=3).

IG-TEM revealed that K75 frequently co-existed with AMBN and AMELX in the small and large vesicles in the ameloblast cell body and in small vesicles of the Tomes' processes (Fig. 8B-G). In contrast LSC primarily contained AMELX signal, whereas K75 and AMBN were in relatively low amounts (Fig. 6D-G). In complement to the cell body IF co-localization analysis, a quantitative co-localization analysis of K75 with AMBN and AMELX in small vesicles of Tomes' process was carried out (Fig. 9B). More than 90% of the small K75-containing vesicles in the Tomes' processes contained AMBN or AMELX, indicating that the majority vesicles in Tomes' process contained more than one protein, which is consistent with earlier studies of AMBN and AMLEX.[63]

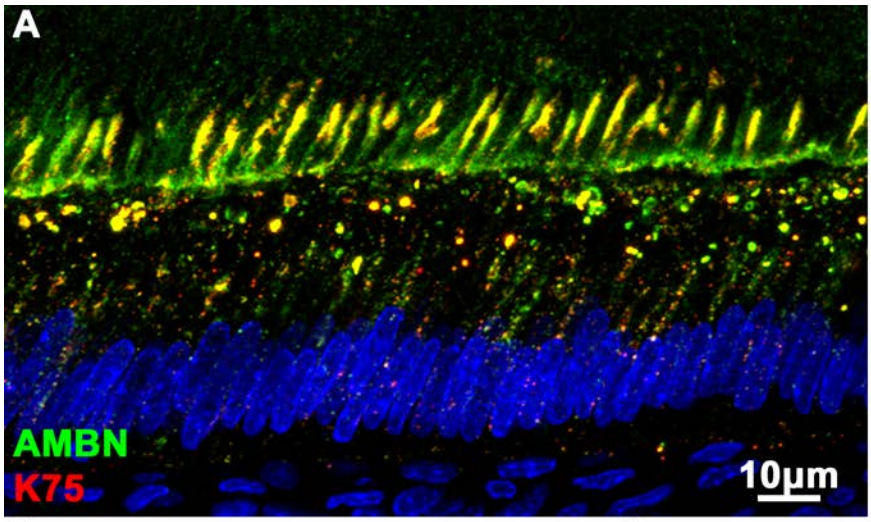

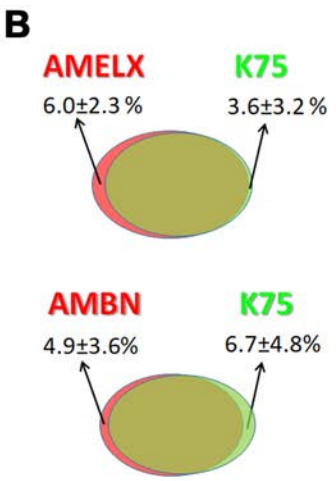

C

	Rat 1	Rat 2	Rat 3	Mean	SD
K75 alone	9%	17%	7%	11%	4%
K75/AMELX	6%	10%	4%	7%	3%
K75/AMBN	27%	33%	27%	29%	3%
K75/AMBN/AMELX	58%	41%	64%	54%	9%
AMELX alone	33%	61%	32%	42%	14%
AMELX/K75*	4%	4%	2%	3%	1%
AMELX/AMBN	29%	17%	38%	28%	9%
AMELX/AMNB/K75	34%	17%	28%	26%	7%
AMBN alone	41%	47%	47%	45%	3%
AMBN/K75	12%	15%	8%	12%	3%
AMBN/AMELX	22%	19%	25%	22%	3%
AMBN/AMELX/K75	25%	19%	19%	21%	3%

D

	Rat 1	Rat 2	Rat 3	Mean	SD
K75/AMELX	95.6%	92.4%	100.0%	96.0%	3.8%
AMELX/K75	94.2%	98.7%	91.6%	94.8%	3.6%
K75/AMBN	97.6%	92.6%	93.1%	94.4%	2.8%
AMBN/K75	89.9%	96.7%	91.7%	92.8%	3.5%

Figure 9. Co-localization of K75 and EMPs in Tomes' process.

(A) Co-labelling of AMBN and K75 in secretory ameloblasts. Please note that these two proteins are highly co-localized in large granules and Tomes' process. (B) Quantitative results of co-localization of AMELX and AMBN with K75 in Tomes' process vesicles under IG-TEM (n=3). (C) Details of IF co-localization analysis in three rats. (D) Details of IG-TEM co-localization analysis in three rats. *AMELX/K75 represent percentage of AMELX signal overlapping with K75 signal, while K75/AMELX indicate percentage of K75 overlapping with AMELX. Similar format is used for AMBN/K75 overlap as well.

4.0 TRAFFICKING OF K75 IN SECRETORY AMELOBLASTS

4.1 CO-LOCALIZATION STUFY OF K75 AND CELLULAR COMPARTMENTS BY IF AND IG-TEM

The co-localization of K75 with AMBN and AMELX in secretory vesicles and in the extracellular space suggest that K75 is co-transported with the EMPs. To gain the insights into the trafficking of K75 in secretory ameloblasts a series of co-localization studies of K75 with different cellular compartment markers were conducted. For comparison, similar co-localization experiments with AMBN, which utilizes the conventional ER-Golgi secretory pathway, were conducted in mice.

4.1.1 Co-localization with ER marker CP1

A diffuse signal of ER marker CP1 was found throughout the ameloblast cytoplasm except for the Tomes' processes (Fig. 10A,E). However, no significant overlap between K75 and CP1 was observed (5.9±1.0%, n=3). Similarly, no K75 label was found inside rER lumen by IG-TEM (Fig. 11A). AMBN, a conventional secretory protein with a signal peptide, had a fairly low level of overlap with CP1 (13.6±3.1%, n=3). While no significant overlap between K75 and CP1 is expected, since K75 is lacking the signal peptide, low co-localization levels of AMBN and CP1

can be due to a very short residence time of AMBN molecules in rER as previously reported[68]. As a result, the possibility that K75 was synthesized in rER cannot be excluded, as it may also have very short residency time in the rER.

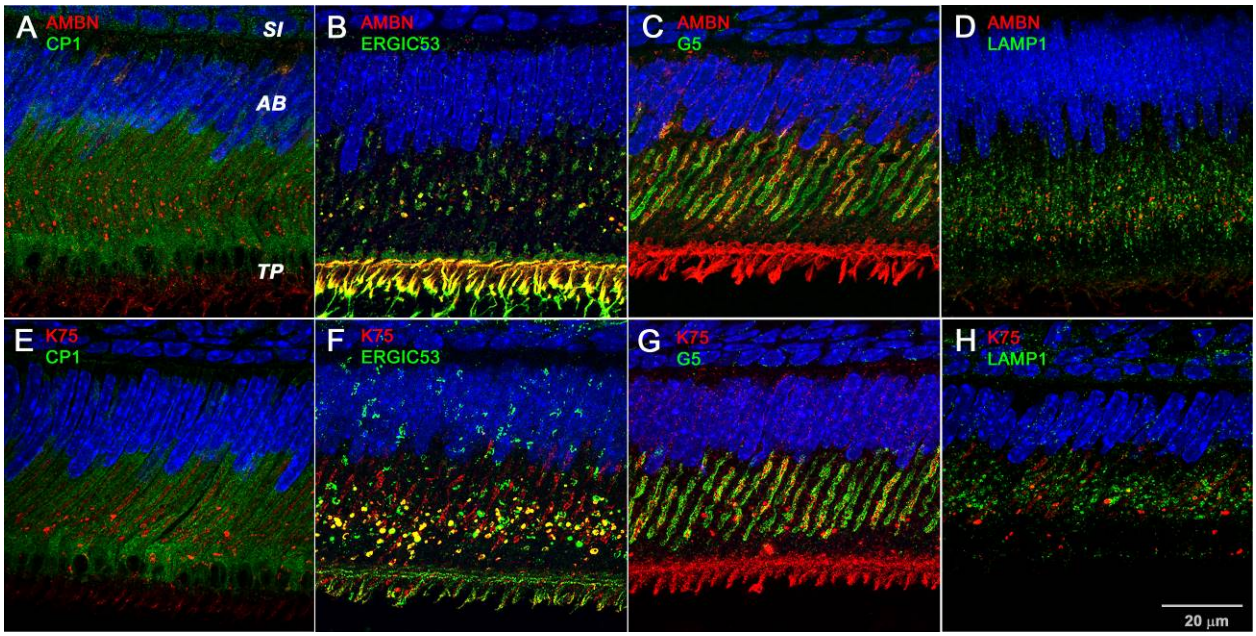

Figure 10. IF Co-localization of AMBN and K75 with different cellular organelle markers in the secretory ameloblasts from 4 weeks old mice.

(A, E) Overlap with ER marker CP1. Note that the overlap is very low for both proteins. (B, F) Overlap with ERGIC marker E53. E53 signal was closely associated with large granules in the ameloblast cell bodies. Noticeably, it was also found in distal portions of ameloblasts, including Tomes' processes. Prominent overlap of K75 and AMBN with E53 was evidenced. (C, G) Overlap with Golgi marker G5. G5 signal appears as two well organized long strips roughly parallel to each other, flanking the core of ameloblast body. Both AMBN and K75 signals organized into bands between the two strips of Golgi complexes in the ameloblast core, partially overlapping with G5. Furthermore, large AMBN and K75 positive vesicles were closely attached to the Golgi, potentially translocating their contents into Golgi for further processing. (D, H) Overlap with lysosome marker LAMP1. LAMP1 signal was present throughout ameloblast cell bodies in the form granules of different shapes and sizes. There was a very limited overlap of K75 with LAMP1. AMBN was slightly more associated with LAMP1 than K75.

4.1.2 Co-localization with ERGIC marker ERGIC53

IF studies revealed that ERGIC marker ERGIC53 (E53) was present in in large granules in the ameloblast cell bodies and as a punctate signal in the cell bodies. Importantly high levels of E53 signal was also observed in the membrane of Tomes' processes (Fig. 10B,F). This observation is very interesting, since Tomes' processes are highly specialized structure where secretory vesicles are released out of ameloblasts whereas ERGIC is thought to be a cellular compartment between rER and Golgi. Considerable degree of overlap was observed between K75 and E53 signal (29.7±6.8% n=3) in the cell body of ameloblasts. Similarly, 26.7±1.7% of AMBN co-localized with E53. In the IF image, almost all K75 containing vesicles co-localized with E53 whereas some E53 positive vesicles did not overlap with K75. Although E53 antibody did not work in IG-TEM experiments, irregularly shaped compartments in the size range of the E53-positive granules in IF images were observed (Fig. 11B,C). The localization of these compartments in the central section of ameloblast between ER and Golgi was also similar to the E53-positive granules. Taken together, these results hint toward the possibility that these are ERGIC. K75 in association with AMBN or AMELX was also found in these compartments by IG-TEM.

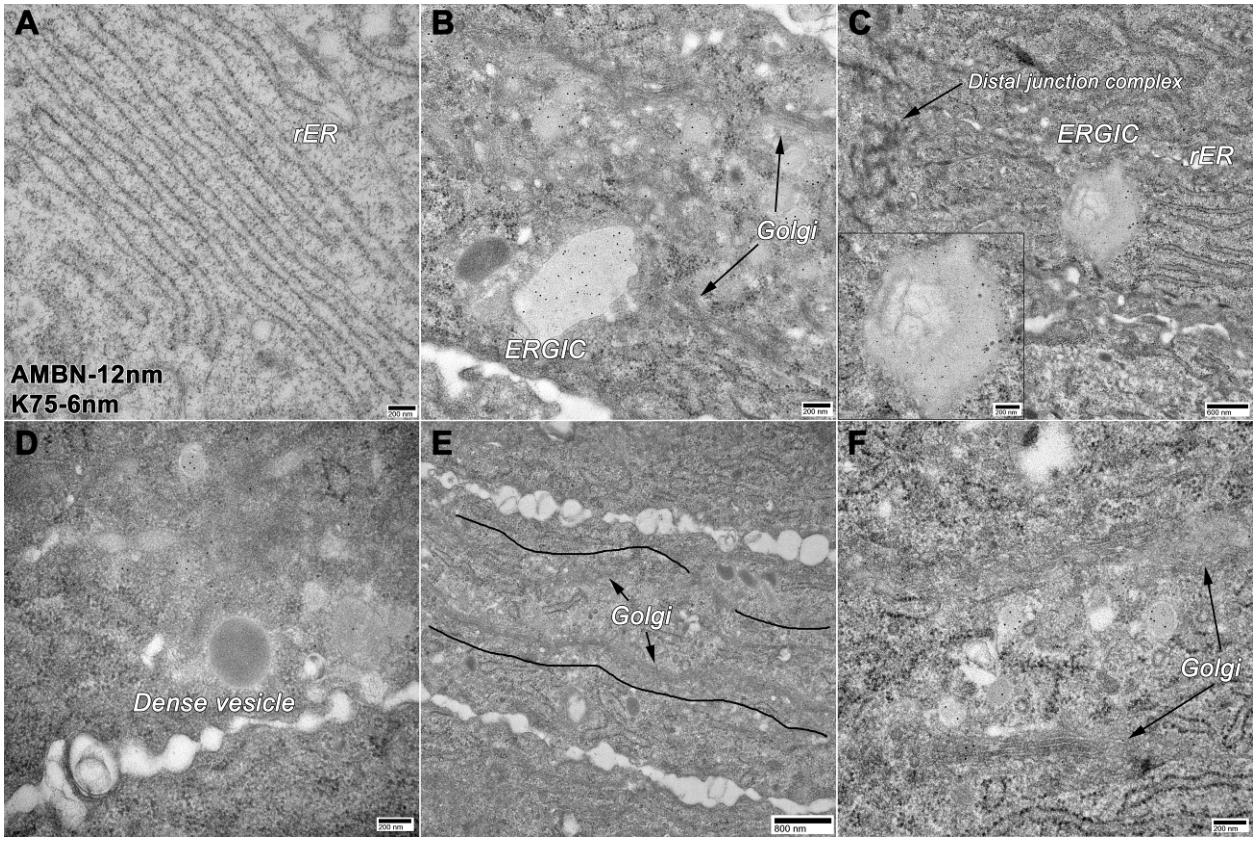

Figure 11. Distribution of AMBN and K75 in different compartments of ameloblasts under IG-TEM.

(A) Under physiological conditions, no obvious labelling was detected in the lumen of rER. (B) An irregular shaped potentially ERGIC containing both AMBN and K75 was in close relationship with central Golgi complex, possibly translocating contents into Golgi complex. (C) A potentially ERGIC located between distal rER rich region and distal junction complex. (D) An un-identified dense vesicle in cytoplasm showing no signals of AMBN and K75 in it. (E, F) Under physiological conditions, central Golgi complex was manifest as two roughly parallel strips of Golgi stacks. Between the two strips of Golgi, abundant small vesicles are shown to contain both AMBN and K75. Some AMBN and K75 signals are also detected in the Golgi cisternae. AMBN and K75 signals are revealed by 12 and 6 nm gold particles.

4.1.3 Co-localization with Golgi marker G5 and GM130

GOLGA5 (G5) was used to track Golgi apparatus cisternae. IF signal of Golgi apparatus in ameloblasts can be elegantly depicted as two long strips roughly parallel to each other, located in the central portion of the ameloblast between the nucleus and the distal junctional complex (Fig. 10C,G). This is in a good agreement with earlier TEM studies, describing the central Golgi complex as two parallel strips of Golgi cisternae running along the ameloblast long axis with rER located between the Golgi strips and the plasma membrane. Earlier ultrastructural studies provide evidence that cis-Golgi in the central portion of ameloblast faces plasma membrane and the trans-Golgi faces the interior[3,13,14]. IF double labeling revealed that both AMBN and K75 had their diffuse form signals streaming just between the two Golgi apparatus strips, and overlapped with the interior trans-Golgi layer. Moreover, AMBN and K75 positive granules, approved to be co-localized with E53, were closely attached to the cis-Golgi surface (Fig. 10C,G). The quantitative co-localization analysis revealed high degree of overlap of K75 (54±16%, n=3) and AMBN (45.3±8%, n=3) with G5. Another Golgi apparatus marker GM130 was also used in the co-localization studies, and it showed generally the same trend as G5.

IG-TEM generally confirmed the IF observations but with more ultrastructural details. Two parallel strips of central Golgi complex are aligned along the long axis of ameloblasts. Each strip comprises several stacks of cisternae. The Golgi cisternae can be several microns long (Fig. 11E). The trans-face of Golgi outlines the cell core, an internal space which is full of small vesicles containing AMBN, K75, and probably some other EMPs (Fig. 1, Fig. 11F). This internal space was associated diffuse signals in IF. Fig. 11B shows a large size compartment, presumed to be ERGIC, in a close proximity to the Golgi apparatus. in the cis face of central Golgi apparatus.

4.1.4 Co-localization with lysosome marker LAMP1 and LAMP2

LAMP1 and LAMP2 signals were found throughout the ameloblast cell bodies in irregular granules or in plaques. Double labeling studies revealed a negligible level (below 10%) of overlap between K75 and LAMP1 (Fig. 10D,H). AMBN overlap with LAMP1 was also low but slightly higher that of K75.

In summary, considerable degrees of overlap were found for K75 and AMBN, with ERGIC and Golgi apparatus. The granular signals of K75 and AMBN showed preferable co-localization with E53 whereas the diffuse signals were more associated with G5 and GM130. Overlap of K75 and AMBN with rER and Lysosome in secretory stage ameloblasts was limited.

4.2 TRAFFICKING INHIBITION STUDY USING BREFELDIN A

BFA is a cellular trafficking inhibitor preventing protein transport from rER to Golgi[72]. Earlier studies of rat secretory ameloblasts treated with BFA revealed that AMBN and AMELX accumulated in rER and their trafficking to the Golgi was blocked[73]. To figure out whether K75 also utilizes conventional trafficking pathway from rER to Golgi, similarly to AMBN, a number of BFA inhibition experiments were conducted. AMBN and K75 distribution in secretory ameloblasts and their co-localizations with rER, ERGIC and Golgi were studied. Animals were injected with BFA dissolved in different solvents intrapritoneally and were euthanized at different time points and processed for IF and IG-TEM studies of the secretory stage ameloblasts.

4.2.1 BFA delivery in DMSO

DMSO is an organosulfur compound which dissolves both polar and nonpolar chemicals. In this study, 0.5mg BFA dissolved in 250 µl DMSO was injected intraperitoneally and the mice were euthanized 1h, 3h and 5h after injection. DMSO is a slow absorbing solvent that even after 5 hours it was still present at the injection site when the mice were sacrificed.

One hour after injection, granules positive for E53 and K75 could still be found, however with less defined boundaries and smaller quantities, which indicated these granules were disappearing (Fig. 12D). The distribution pattern of AMBN became less organized than in untreated ameloblasts, yet a considerable overlap with E53 could still be seen at this time point (Fig. 12A). Importantly, IF co-localization studies of K75 and AMBN with ER marker CP1 revealed a significant overlap between CP1 and AMBN, while no obvious co-localization was observed between K75 and CP1 (Fig. 13A,D). The accumulation of AMBN in rER after BFA treatment is characteristic for conventional secretory proteins utilizing rER-Golgi pathway. In contrast, the low co-localization of K75 and CP1 after BFA treatment implied a different synthesis site of K75 other than rER. Golgi apparatus one hour after injection lost its typical double strip appearance and became dispersed in the cytoplasm (Fig. 14A,D). At this time point, both AMBN and K75 still showed some overlap with G5 signal, probably because the proteins produced previously were still transported through Golgi apparatus.

Three hours after injection, no large E53 positive granules could be detected (Fig. 12B,E). Instead, diffuse E53 signal was observed throughout the cell. AMBN still showed some overlap with E53 and CP1. Meanwhile K75 signal was isolated from both E53 and CP1. At three hours after injection, Golgi apparatus started to recover and regain its morphology (Fig. 14 B,E). An interesting phenomenon was found regarding the relative position of AMBN and Golgi

apparatus. We noticed that G5 was in the central region of the cytoplasm while high levels AMBN signal were detected in the peripheral space (Fig. 14B). The overlap between these two was very limited, which meant the newly synthesized AMBN was trapped in peripheral rER and could not make its way to Golgi apparatus. In contrast, K75 revealed a totally different distribution pattern. It was concentrated in the internal space between the double strips of Golgi apparatus and showed strong co-localization with G5 signal (Fig. 14E). This observation suggested that K75 entered Golgi apparatus via an unknown pathway when the conventional rER-Golgi trafficking route was blocked by BFA.

Five hours after injection, the overall distribution pattern of all markers remained similar to those at three hours, whereas all signal strengths became weaker and more dispersed (Fig. 12C,F, 13C,F, 14C,F).

To test whether DMSO alone could cause changes in organelle and protein distribution, same amount of DMSO was injected as vehicle control, and the mice were sacrificed after 3 hours. Substantial effects were observed in DMSO treated ameloblasts(Fig. 15,16B,F). Most of the E53 granules were disappeared, and distributions of AMBN and K75 were also dramatically changed. CP1 and G5 signals seemed to be just fine.

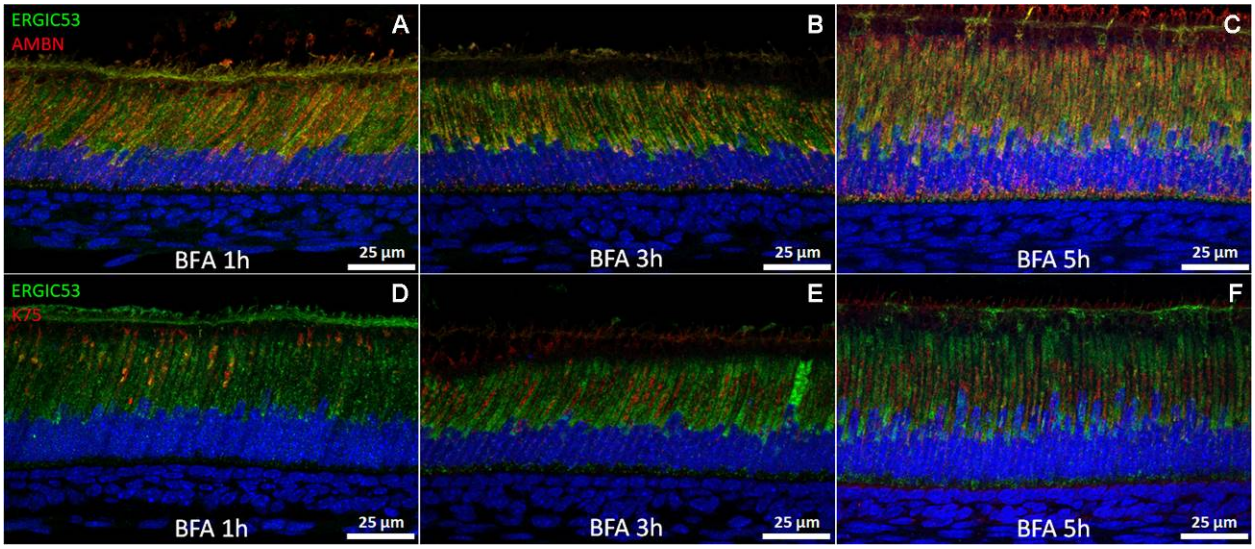

Figure 12. Effects of BFA dissolved in DMSO on ERGIC organization and AMBN and K75 distribution 1, 3 and 5 hours after injection.

(A-C) Co-labelling of E53 and AMBN at 1, 3 and 5-hour points. AMBN signal became diffused in all three time points, yet still showed considerable overlap with E53. (D-F) Co-labelling of E53 and K75 at 1, 3 and 5 hour points. At 1 hour, granules positive for E53 and K75 were becoming blur in their boundaries. At 3 and 5 hours, granules totally disappeared and K75 signal showed a central band form.

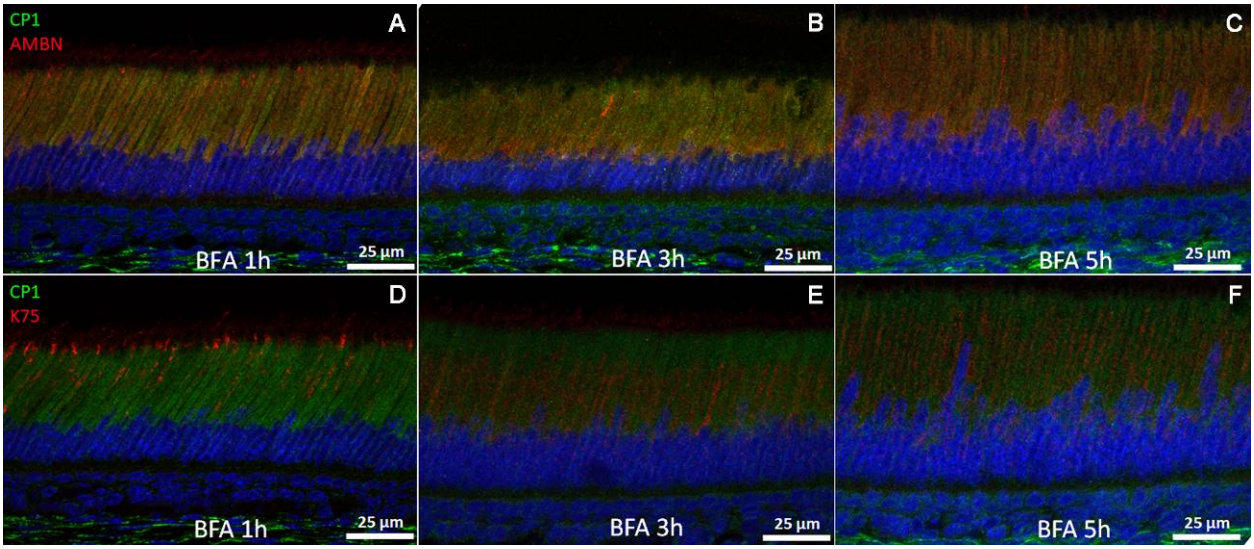

Figure 13. Effects of BFA dissolved in DMSO on ER organization and AMBN and K75 distribution 1, 3 and 5 hours after injection.

(A-C) Co-labelling of CP1 and AMBN at 1, 3 and 5 hour points. Diffuse AMBN signal showed considerable overlap with ER marker CP1. (D-F) Co-labelling of CP1 and K75 at 1, 3 and 5 hour points. The overlap of K75 and CP1 was always low from 1 to 5 hour points.

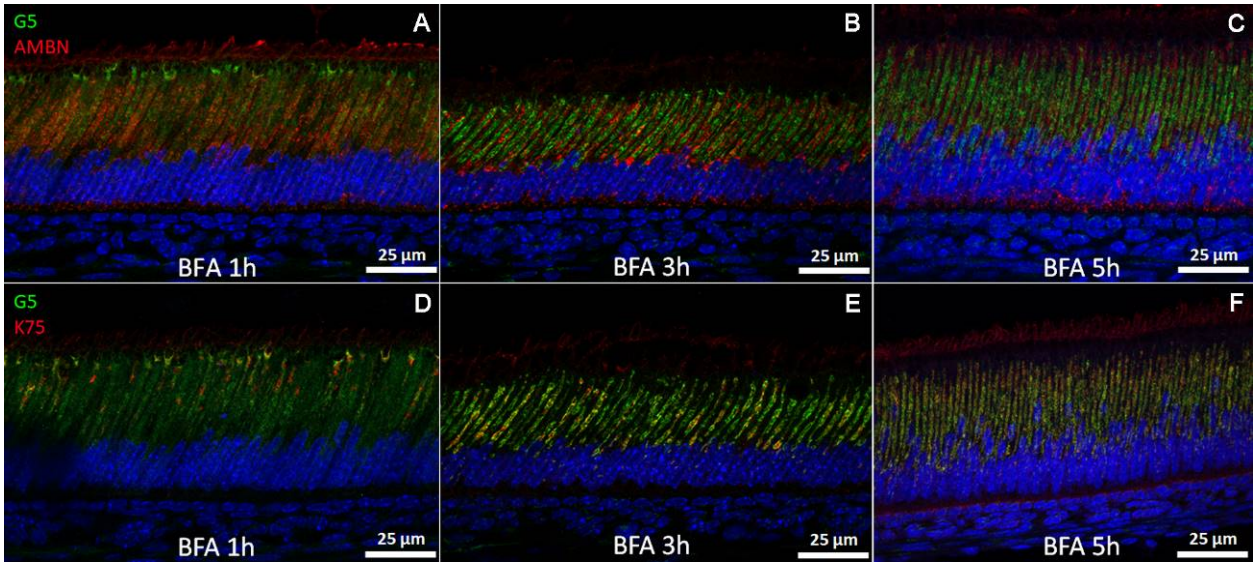

Figure 14. Effects of BFA dissolved in DMSO on Golgi organization and AMBN and K75 distribution, 1, 3 and 5 hours after injection.

(A-C) Co-labelling of G5 and AMBN at 1, 3 and 5 hour points. At 1 hour, AMBN signal became diffuse throughout the cytoplasm. At 3 hour, AMBN signal was majorly located in the peripheral region, isolated from central Golgi complex. At 5 hour, same pattern as that in 3 hour still existed. (D-F) Co-labelling of G5 and K75 at 1, 3 and 5 hour points. Different from that of AMBN, K75 signal manifest considerable overlap with central Golgi complex.

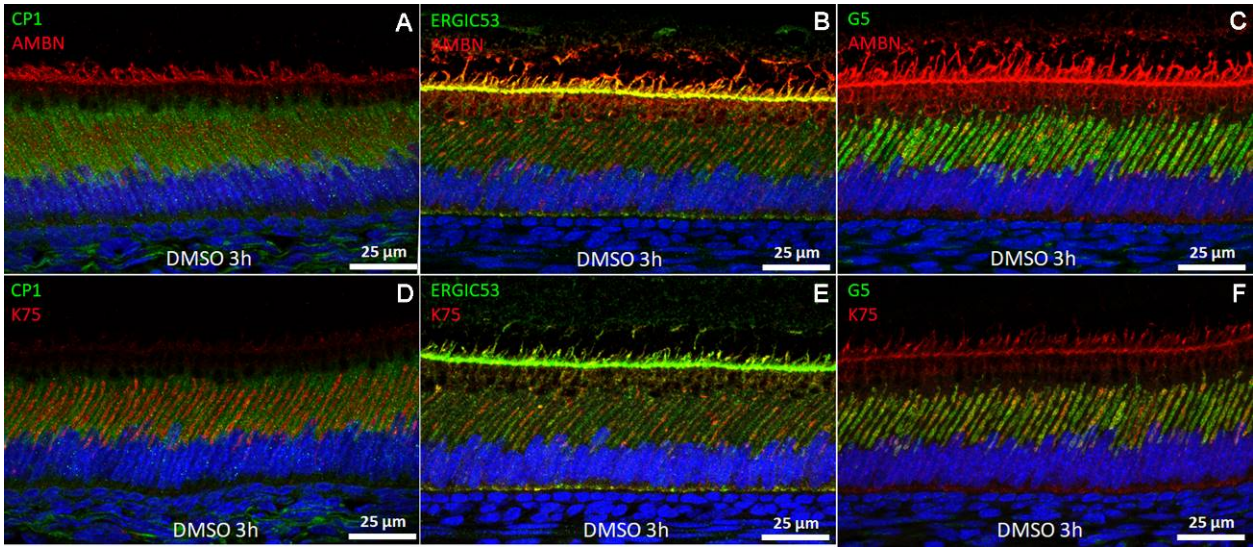

Figure 15. Effects of DMSO on AMBN and K75 distribution after 3 hours.

(A, D) Co-labelling of CP1 with AMBN and K75 at 3 hours. (B, E) Co-labelling of E53 with AMBN and K75 at 3 hours. (C, F) Co-labelling of G5 with AMBN and K75 at 3 hours.

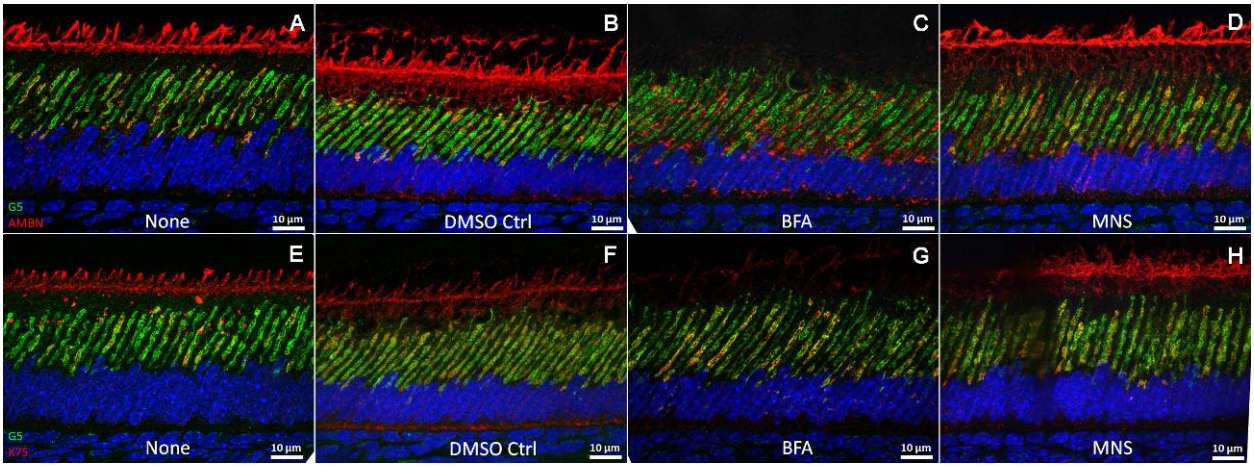

Figure 16. Effects of BFA and MNS in DMSO solvent on AMBN and K75 distribution, co-labelled with G5 after 3 hours.

(A, E) Mice ameloblasts without any treatment. (B, F) Mice ameloblasts treated with only DMSO. (C, G) Mice ameloblasts treated with BFA in DMSO after 3 hours. (D, H) Mice ameloblasts treated with MNS in DMSO after 2.5 hours. Compared with none-treated, DMSO Ctrl group had AMBN and K75 granules disappeared whereas the central band signal remained.

4.2.2 BFA delivery in ethanol

Since DMSO alone could cause the disappearance of ERGIC (Fig. 15, 16B,F) and affect the trafficking of AMBN and K75, a harmless solvent is desired. In the next series of experiments, the mice were injected with BFA dissolved in 30% ethanol. Animals injected with 30% ethanol only (vehicle) were used as controls. As soon as one hour after injection, all injected solution was absorbed. No significant differences in distribution and localization of AMBN, K75 and organelle markers were observed between the vehicle controls and untreated samples. In contrast to DMSO, which absorbed slowly, the effects of BFA in 30% ethanol was manifested prominently just an hour after injection.

One hour after injection, AMBN signal was enriched in the distal part, where rER rich zone was located, and periphery of ameloblasts (Fig. 17A, 18A, 19A, 20A, 21B, 22E,G). AMBN exhibited high degree of overlap with rER (Fig. 17A, 22E). In contrast, no obvious change in co-localization of K75 and CP1 was observed (Fig. 17D, 22F). Although the morphology of Golgi apparatus was somewhat disturbed, parallel Golgi strips were still located in the central region of cytoplasm and exhibited a sizable overlap with K75 (Fig. 19D, 21D, 22H). Meanwhile, almost no overlap was detected between AMBN and G5 (Fig. 19A, 21B, 22G). These results were consistent with the results obtained when DMSO solvent was used, showing accumulation of AMBN in rER, and persistent existence of K75 in Golgi.

Two hours after injection, the amount of AMBN signal appeared to be reduced compared to one hour. AMBN still showed limited overlap with Golgi apparatus (Fig. 19B). Three hours after injection, AMBN partially regained its normal distribution pattern. Some AMBN signal was relocated between the two Golgi strips and exhibited a substantial overlap with G5 (Fig. 19C); E53 and AMBN positive granules also started to reappear (Fig. 18C) and the co-localization with

CP1 decreased (Fig. 17C). These results indicated that between 2 and 3 hours after injection, the inhibitory effects of BFA diminished. rER to Golgi trafficking pathway began to recover, and AMBN accumulated in rER was able to translocate into Golgi apparatus again.

In contrast, high degree of co-localization of K75 and Golgi was not affected by BFA treatment. One and two hours after injection, K75 was still located between the two strips of Golgi apparatus. However, instead of being a narrow band, K75 signal was slightly broadened (Fig. 19D,E). After three hours, trafficking of K75 was majorly back to normal (Fig. 19F). Large granules, presumably ERGIC, showed up again.

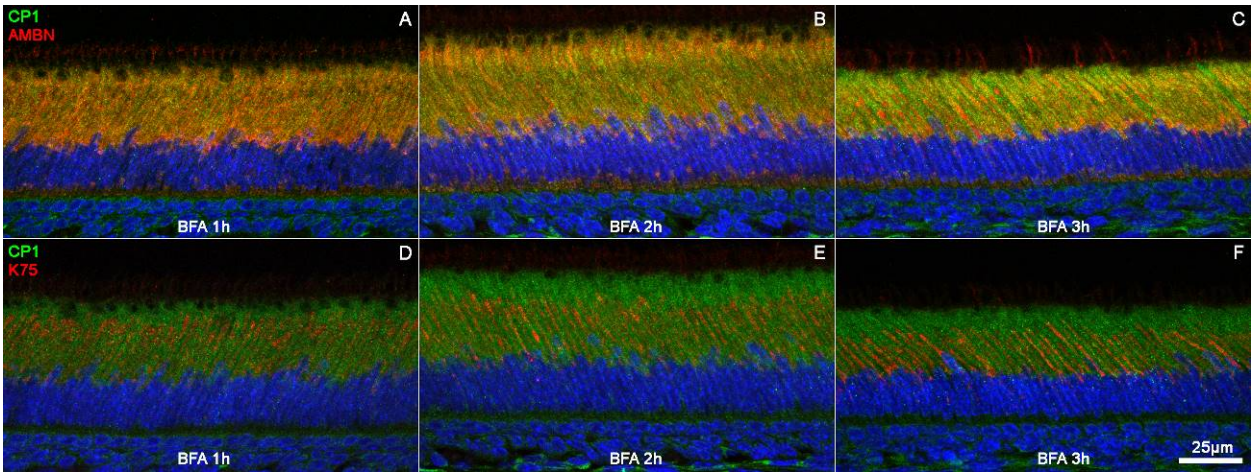

Figure 17. Effects of BFA dissolved in ethanol on ER organization and AMBN and K75 distribution, co-labelled with CP1 1, 2 and 3 hours after injection.

(A-C) Co-labelling of CP1 and AMBN at 1, 2 and 3 hour points. Diffuse AMBN signal showed prominent overlap with ER marker CP1 at all three time points, although the tendency seemed decrease at 3 hour. (D-F) Co-labelling of CP1 and K75 at 1, 2 and 3 hour points. K75 showed limited overlap with CP1 in all time points.

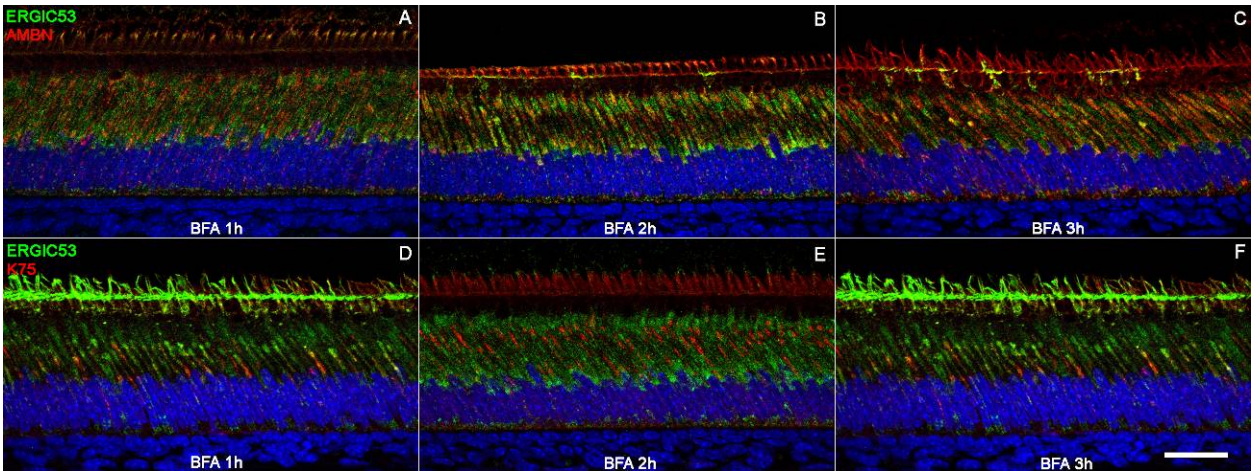

Figure 18. Effects of BFA dissolved in ethanol on ERGIC organization and AMBN and K75 distribution, co-labelled with CP1 1, 2 and 3 hours after injection.

(A-C) Co-labelling of CP1 and AMBN at 1, 2 and 3 hour points. At 1 hour, E53 and AMBN positive granules were disappeared. At 2 and 3 hour, diffuse AMBN was still associated with E53 signal. At 3 hour, E53 and AMBN positive granules started to show up again. (D-F) Co-labelling of CP1 and K75 at 1, 2 and 3 hour points.

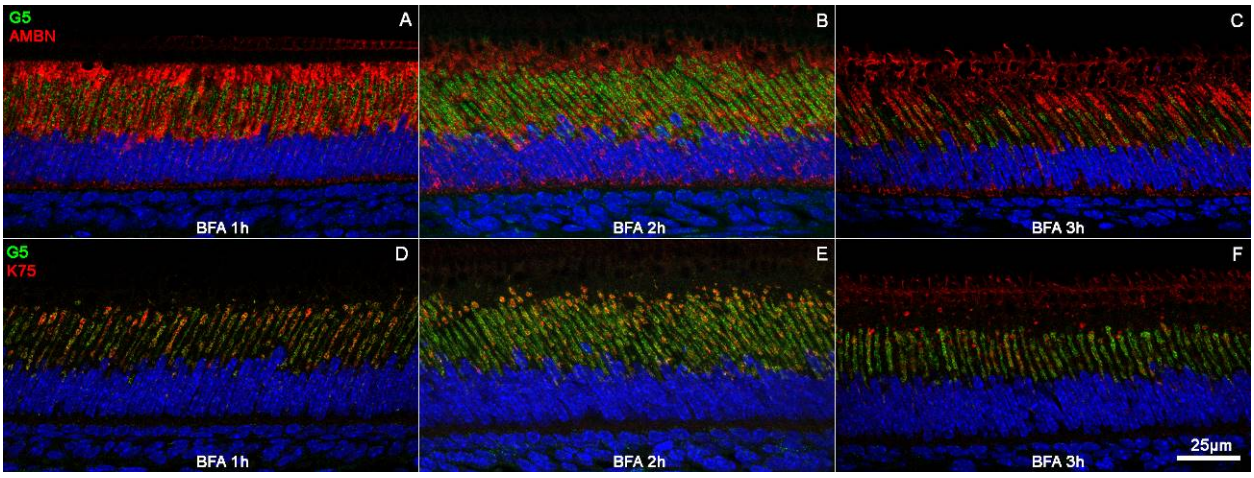

Figure 19. Effects of BFA dissolved in ethanol on Golgi organization and AMBN and K75 distribution, co-labelled with G5 1, 2 and 3 hours after injection.

(A-C) Co-labelling of G5 and AMBN at 1, 2 and 3 hour points. AMBN showed obvious isolation from G5 at 1 and 2 hours. At 3 hour, AMBN was partially recovered, evidenced by more central distribution and re-appearance of AMBN granules. (D-F) Co-labelling of G5 and K75 at 1, 2 and 3 hour points. K75 positive granules disappeared at 1 and 2 hours while central K75 signal still showed considerable overlap with G5. At 3 hour, K75 signal was back to normal.

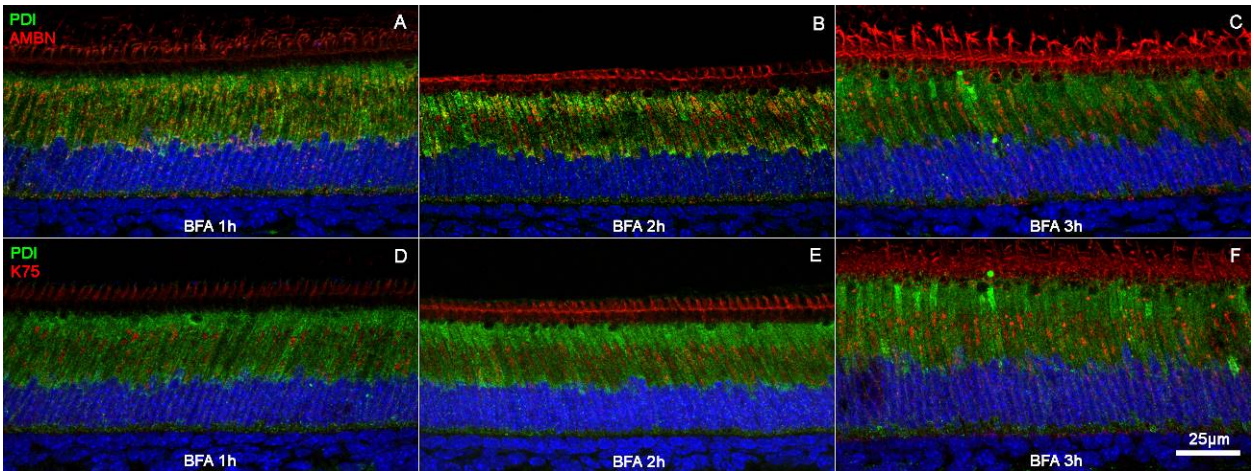

Figure 20. Effects of ethanol dissolved BFA on AMBN and K75 distribution, co-labelled with PDI after 1, 2 and 3 hours.

(A-C) Co-labelling of PDI and AMBN at 1, 2 and 3 hour points. AMBN also showed elevated overlap with PDI, however not as prominent as CP1. (D-F) Co-labelling of PDI and K75 at 1, 2 and 3 hour points. Co-localization of K75 and PDI was always in a low level.

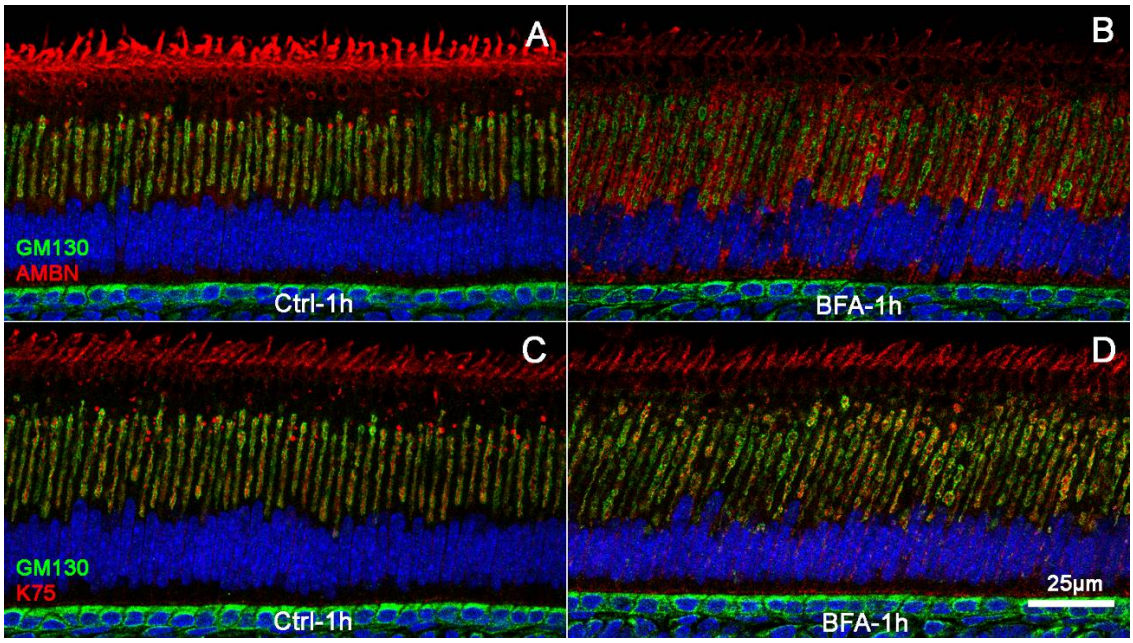

Figure 21. Effects of ethanol dissolved BFA on AMBN and K75 distribution, co-labelled with GM130 after 1hour.

(A, C) Co-labelling of AMBN and K75 with GM130 at 1 hour for vehicle control group. (B, D) Co-labelling of AMBN and K75 with GM130 at 1 hour for BFA group.

To better understand the changes in co-localization of K75 and AMBN with the organelle markers, a quantitative analysis was carried out at one hour time point. This analysis was carried out only on the ameloblast cell body region excluding the Tomes' processes. The co-localization analysis in the control group showed that 14±2.5% of AMBN and 6±1% of K75 co-localized with rER (Fig. 22I). While no significant overlap between K75 and CP1 is expected, since K75 is lacking the signal peptide, low co-localization levels of AMBN and CP1 can be due to a very short residence time of AMBN molecules in rER as it was previously reported[68]. In contrast substantial levels of co-localization of K75 (54±16%) and AMBN (45.3±8%) with G5 were found (Fig. 22J). In the BFA treated group, the co-localization pattern of AMBN changed dramatically. AMBN signal associated with the central Golgi complex decreased significantly (8.5±2%, $p<0.01$) while its overlap with the peripheral rER increased significantly (30±5%, $p<0.01$). These results demonstrated that the disruption of rER-Golgi transport by BFA leads to the accumulation of AMBN in rER and its depletion form Golgi, which is anticipated for an extracellular protein secreted via the classical rER-Golgi dependent pathway[45,74]. The treatment with BFA, however, had a more limited effect on the localization of K75. Co-localization of K75 and CP1 in the treatment group remained at low levels comparable to the control (10±1%). In contrast, no significant changes existed in co-localization of K75 and G5 between the control and treatment groups (41±14% vs. 54±16%; $p=0.34$). In the untreated samples 22±2% of AMBN and 30±7% of K75 overlapped with E53. One hour after the BFA injection, the overlap between E53 and AMBN did not change significantly (22±2% vs. 27±11%, $p=0.53$), while a significant reduction in K75 co-localization with E53 was observed (30±7% vs. 10±2%; $p<0.05$) (Fig. 23). The fact that the overlap between AMBN and E53 did not change, while the E53 positive granules disappeared might indicate that E53 accumulates on the rER membranes, and since rER

contained large amounts of AMBN the overall co-localization percentages did not change. Nevertheless, the fact that the overlap between K75 and E53 significantly decreased while co-localization of K75 and G5 remained statistically unchanged pointed toward the possibility that, in addition to ERGIC-Golgi trafficking route for K75, there is another unknown translocation mechanism.

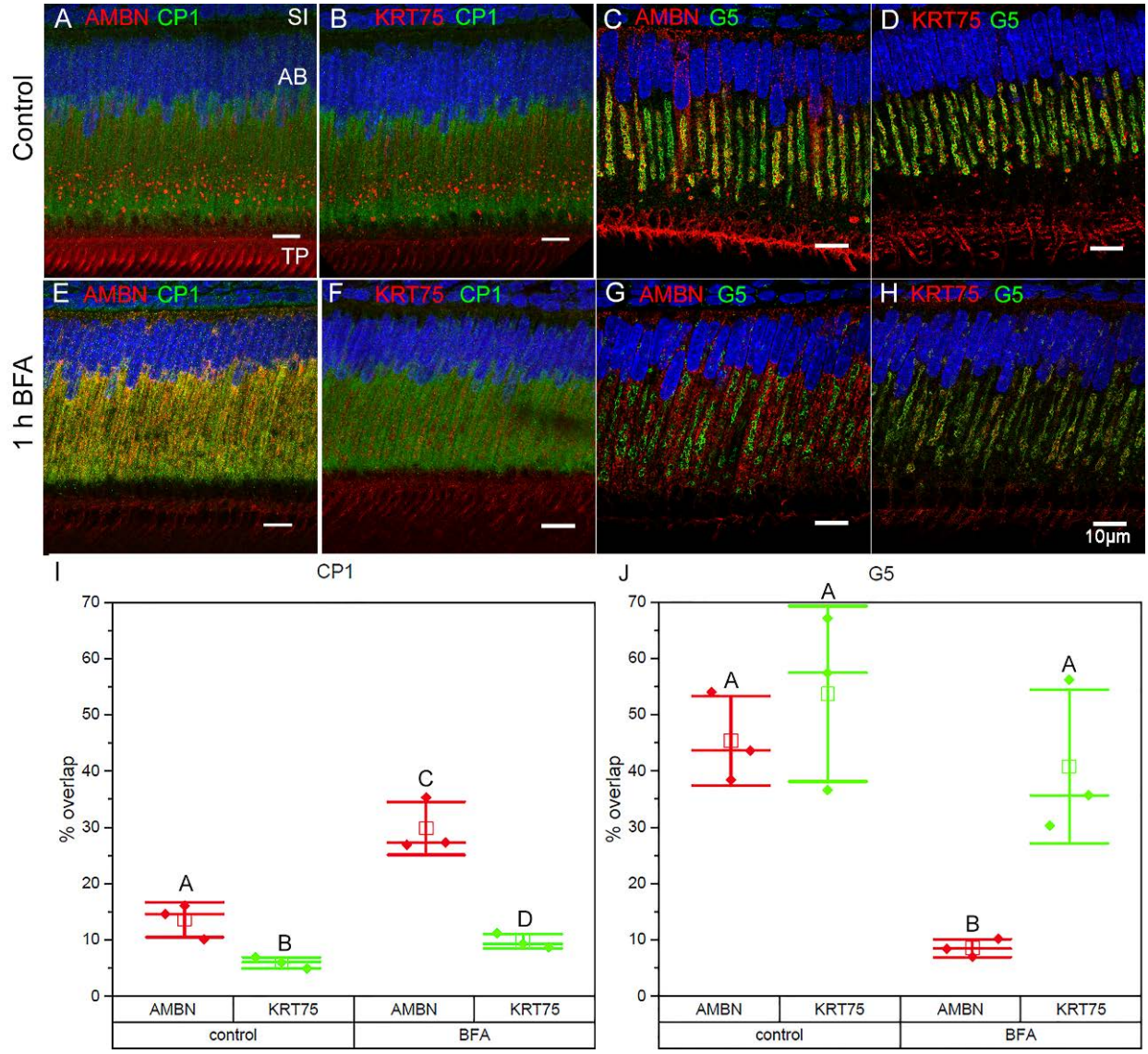

Figure 22. IF analysis of secretory ameloblasts from 4-week old mouse incisors after BFA treatment. (A-D) One hour after the vehicle injection. (E-H) One hour after BFA(ethanol) injection. (I, J) Overlap of AMBN and K75 with CP1 and G5 in vehicle control and BFA groups. Filled diamonds represent the values of the overlap

(%). Open squares represent mean and the central crossbars represent median values, the end crossbars represent SD. Significant differences ($p \leq 0.05$) existed between groups marked by different letters. N=3.

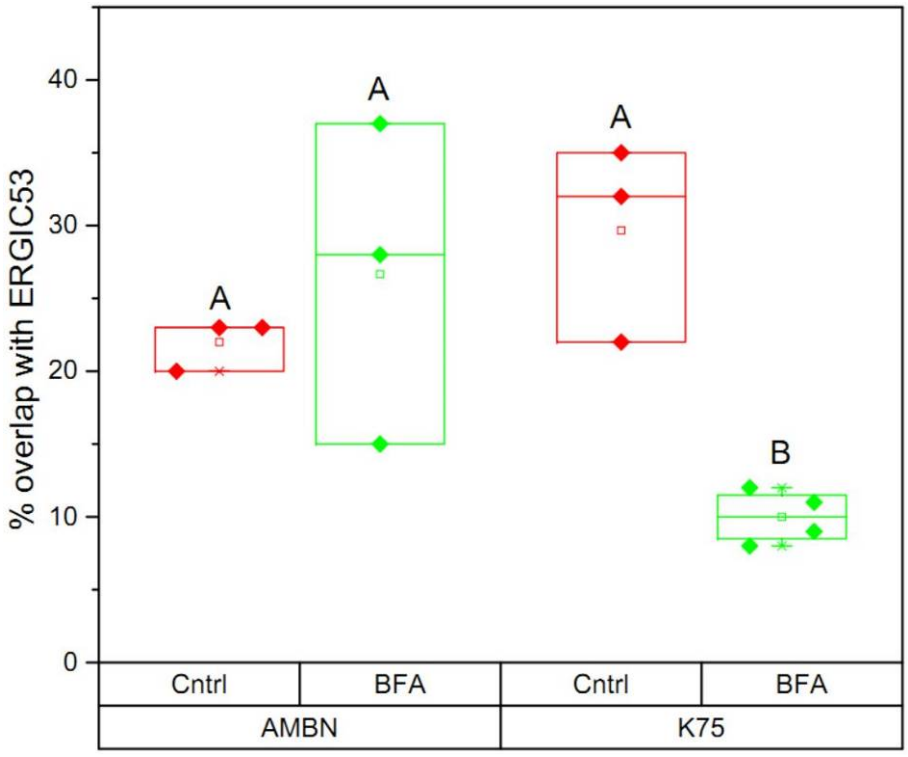

Figure 23. Effects of BFA on the co-localization of AMBN and K75 with E53.

Although ERGIC granules dispersed, the overlap percentage of AMBN and E53 did not change significantly after BFA treatment. However, the co-localization of K75 with E53 dropped significantly after BFA treatment. Significant differences ($p \leq 0.05$) existed between groups marked by different letters. N=3.

4.2.3 BFA delivery in PBS

The effects of BFA on the intracellular trafficking in the mouse secretory ameloblasts were also studied with PBS as the solvent. It is worth noting that when stock solution of BFA in DMSO was diluted in PBS, it became cloudy. However, based on the experimental results, the cloudiness did not seem to affect its absorption. The secretory ameloblasts were examined 15, 30, and 60 min after BFA injection and the vehicle controls were examined 60 min after

injection. As early as 15 min after BFA injection, we could already see the accumulation of AMBN (Fig. 24C, 25C, 26B) and the decreased quantities of granules positive for E53 (Fig. 24C,D). Thirty minutes after injection, these ERGIC granules could not be found anymore. Instead, punctate E53 signal dispersed throughout the ameloblast and its overall strength decreased (Fig. 24E,F). It was also noticed that E53 in the Tomes' process region remained relatively stable and AMBN was still trapped in the peripheral area at this time point. At 60 min point, the AMBN trafficking started to recover. In many ameloblasts, AMBN signal had become more concentrated in the central Golgi complex and a few granules resembling ERGIC could be seen again (Fig. 24G). Compared to 30 min when K75 had a more swollen central band, K75 signal at 60 min point also restored its normal appearance. Meanwhile E53 manifest a slower manner to recover. The E53 signals at 60 min point was located in the central region, where presumably Golgi apparatus exists, and showed overlap with both AMBN and K75 (Fig. 24G,H), probably because the E53 translocated into Golgi had not been recycled yet.

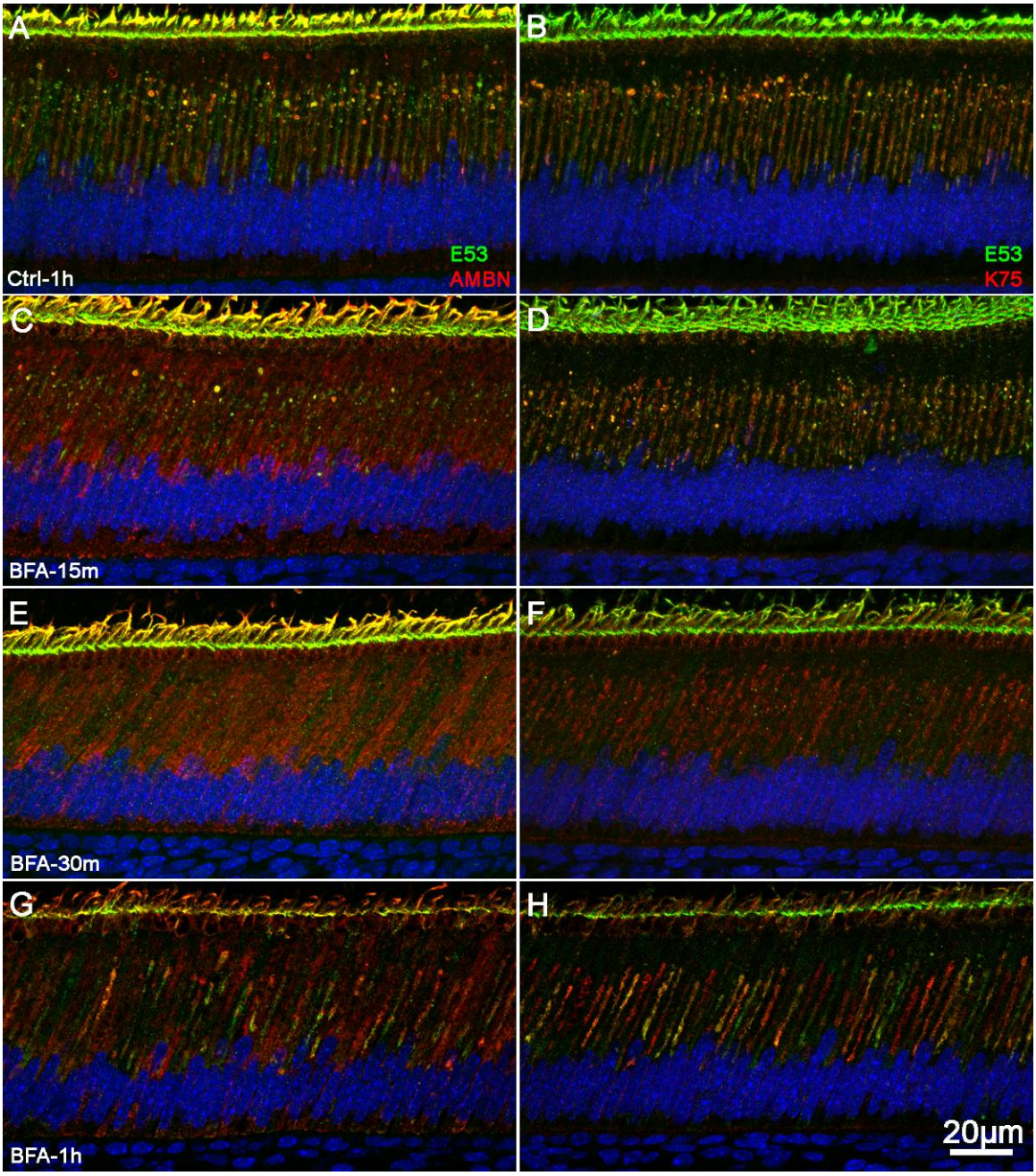

Figure 24. Effects of BFA in PBS on AMBN and K75 distribution, co-labelled with E53.

(A, C, E, G) Co-labelling of E53 and AMBN for vehicle control and BFA in PBS at 15, 30 and 60 minutes. At 15min, the number of ERGIC granule decreased, and they completely disappeared at 30min. Partial recovery was seen at 1 hour. AMBN signal became diffuse after the treatment. (B, D, F, H) Co-labelling of E53 and K75 for vehicle control and BFA in PBS at 15, 30 and 60 minutes. Unlike AMBN, K75 signal did not become diffuse

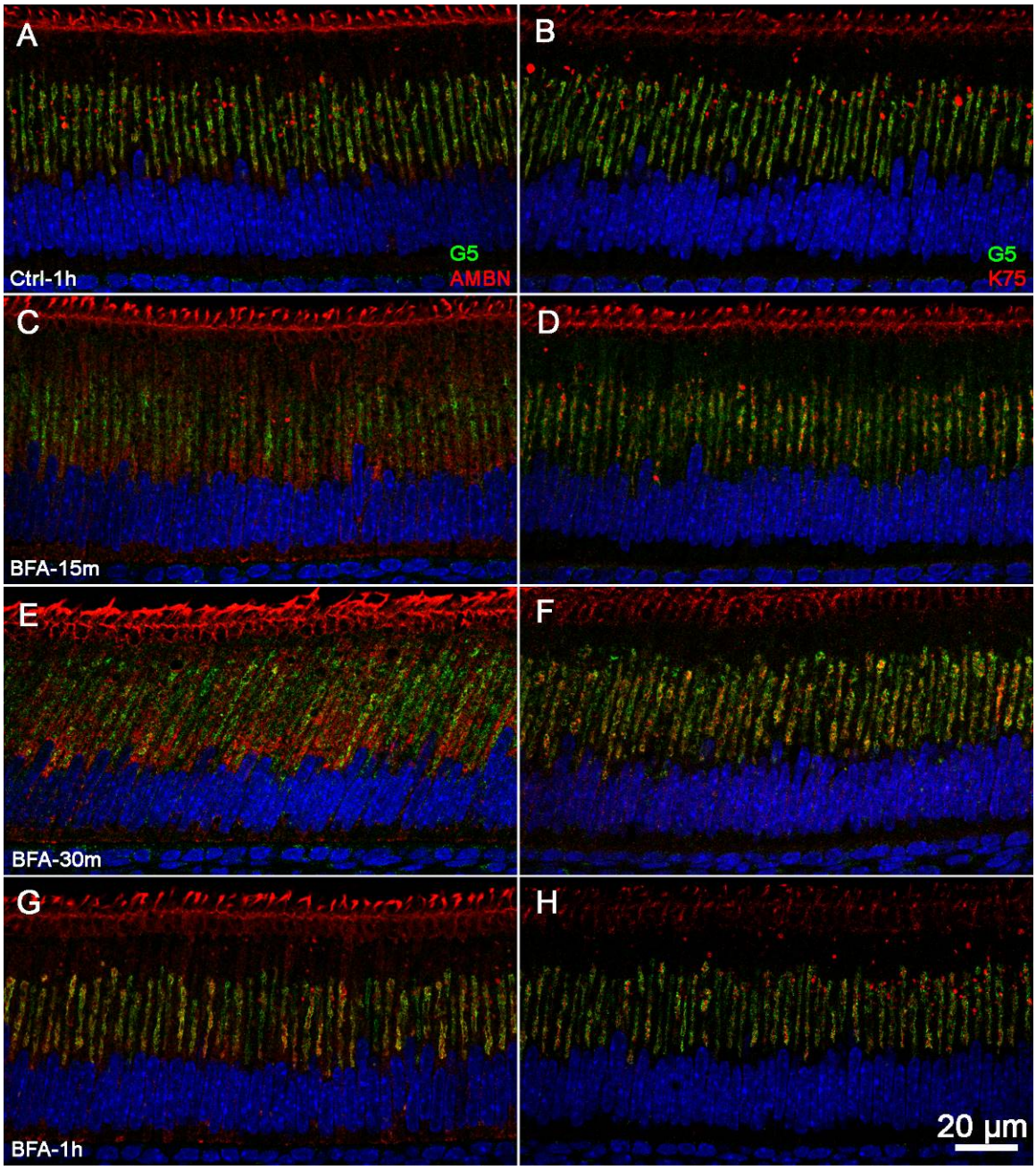

Figure 25. Effects of BFA in PBS on AMBN and K75 distribution, co-labelled with G5.

(A, C, E, G) Co-labelling of G5 and AMBN for vehicle control and BFA in PBS at 15, 30 and 60 minutes. (B, D, F, H) Co-labelling of G5 and K75 for vehicle control and BFA in PBS at 15, 30 and 60 minutes.

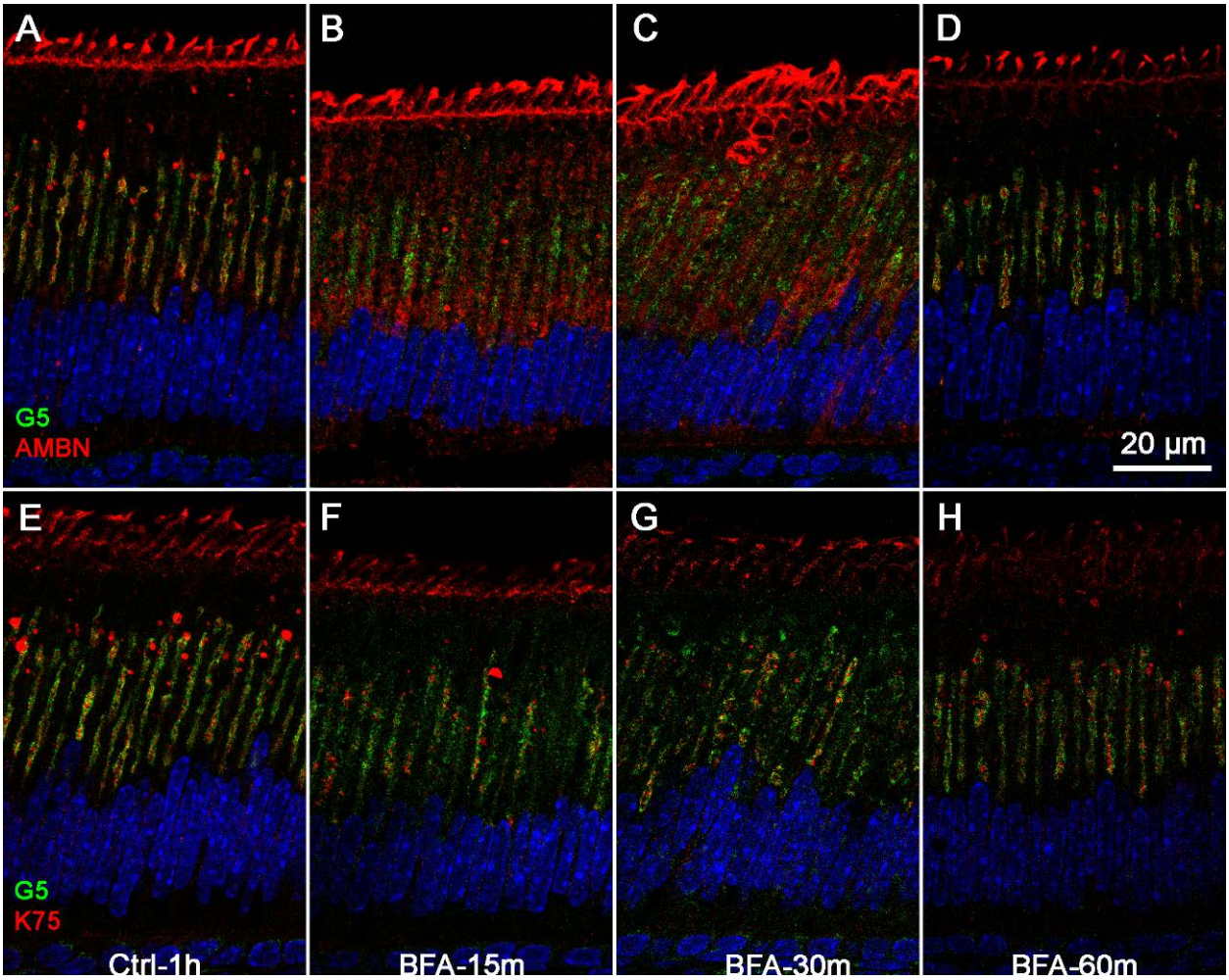

Figure 26. Effects of BFA in PBS on AMBN and K75 distribution, co-labelled with G5 under higher magnification. (A-D) Co-labelling of G5 and AMBN for vehicle control and BFA in PBS at 15, 30 and 60 minutes. (E-H) Co-labelling of G5 and K75 for vehicle control and BFA in PBS at 15, 30 and 60 minutes.

Taken together these results indicate, BFA treatment successfully blocked the conventional rER-Golgi trafficking pathway which is used by AMBN. However, K75 trafficking seemed to be insensitive to the blockage by BFA, indicating that it might utilize a novel UPS pathway. Although three BFA solvents used in this section showed different rates of absorption and some other subtle differences, the same overall responses strengthened our hypothesis.

4.3 TRAFFICKING INHIBITION STUDY USING H89

H-89 is a protein kinase A inhibitor commonly used in cellular trafficking studies in vitro. However, the actual role it plays is still not very clear[75]. Previous studies showed that H-89 could inhibit membrane budding from Trans-Golgi to cell surface[76,77], Gβγ mediated Golgi breakdown[78], ER to Golgi transport[79,80], and induce Golgi disassembly[81]. To verify our previous hypothesis that K75 was not synthesized in rER, we therefore tried to use H-89 to block the conventional protein trafficking out of rER in vivo. To our surprise, the effects of H-89 seemed to be quite different from that of BFA regarding the blockage of ER-Golgi trafficking. While after BFA treatment CP1 signal became more diffuse, CP1 signal appeared as punctate spots in H-89 treated ameloblasts (Fig. 27A,C). At the same time, H-89 lead to a modest inhibition of AMBN trafficking when injected at 5 mg per mouse. In many ameloblasts AMBN signal was detected throughout the cell body (Fig. 27B). At a lower dose of 0.5 mg H-89 per animal, no obvious changes could be observed for AMBN at 1, 2 and 3 hour points (Fig. 28A-C). However, there were some differences in K75 distribution compared with control group one hour after injection. The large size granules positive for K75 and E53 disappeared whereas the central K75 signal band was still present and highly associated with G5 (Fig. 29D). At the later time points K75 distribution was back to normal. Thus, H-89 seemed to partially inhibit AMBN trafficking out of ER at high concentration. It might also specifically inhibited translocation of K75 to ERGIC whereas AMBN translocation to ERGIC was not affected. If this is true, K75 was able to translocate into Golgi complex bypassing ERGIC, similar to what happened after BFA treatment. Another interesting finding when screening the early and late secretory ameloblasts of H-89 treated mouse incisor was that early secretory ameloblasts seemed to have more number of E53 positive granules than those of late secretory ameloblasts (Fig. 30), suggesting the effects of H-

89 might be stage dependent. It should be noted that only a limited number of experiments was performed with H-89 and they need to be repeated and verified.

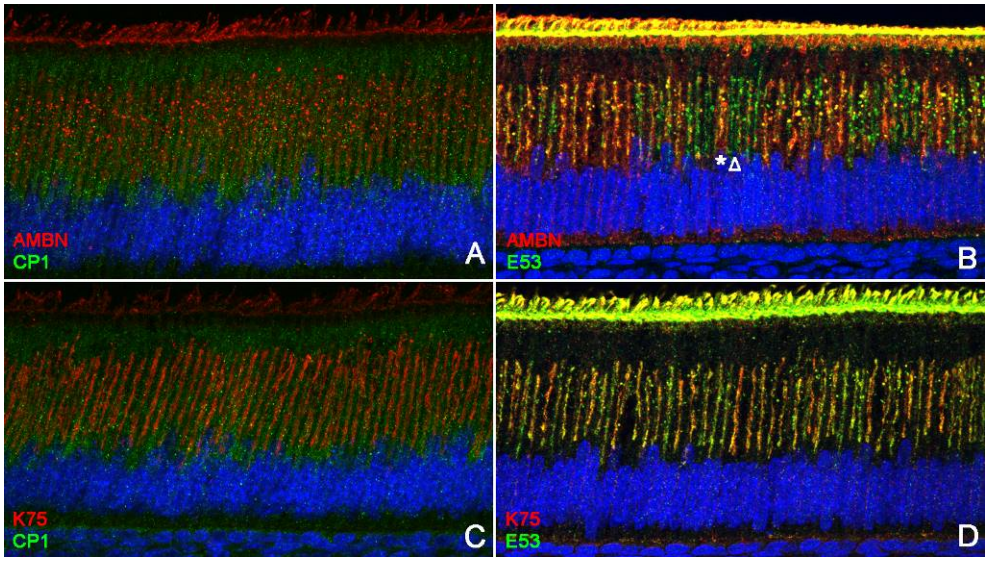

Figure 27. Effects of 5mg H-89 in ethanol on AMBN and K75 distribution.

Five mg H-89 was injected for each mouse, the animal died after around 40m and mandibles were collected for IF staining. (A, C) Co-labelling of AMBN and K75 with CP1. (B, D) Co-labelling of AMBN and K75 with E53. Asterisk showed an ameloblast with partial AMBN trafficking inhibition and triangle pointed to adjacent ameloblast without diffuse AMBN signal in cytoplasm.

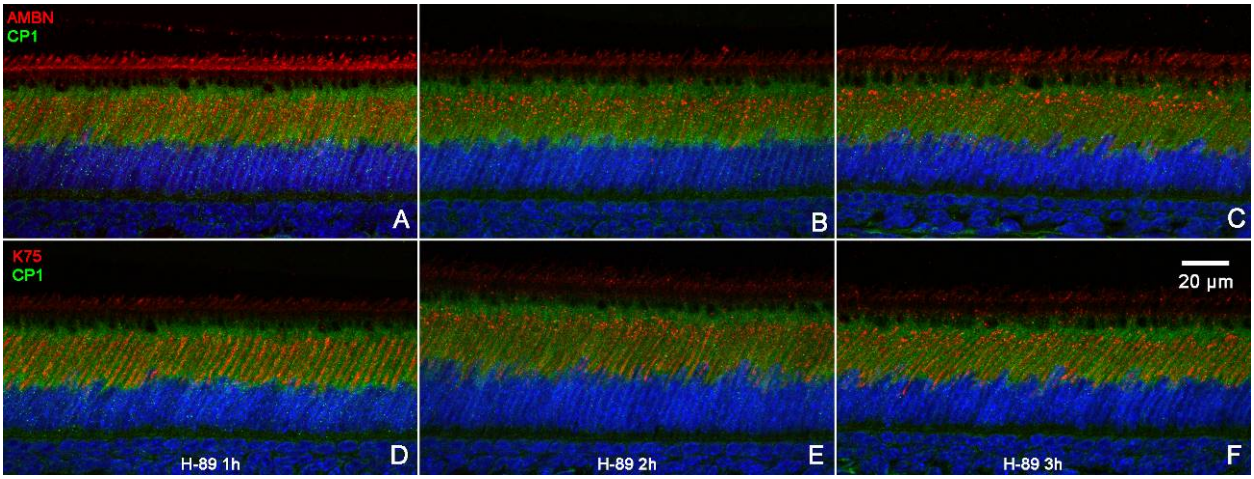

Figure 28. Effects of 0.5mg H-89 in ethanol on AMBN and K75 distribution, co-labelled with CP1 after 1, 2 and 3 hours.

(A-C) Co-labelling of CP1 and AMBN at 1, 2 and 3 hour points. (D-F) Co-labelling of CP1 and K75 at 1, 2 and 3 hour points.

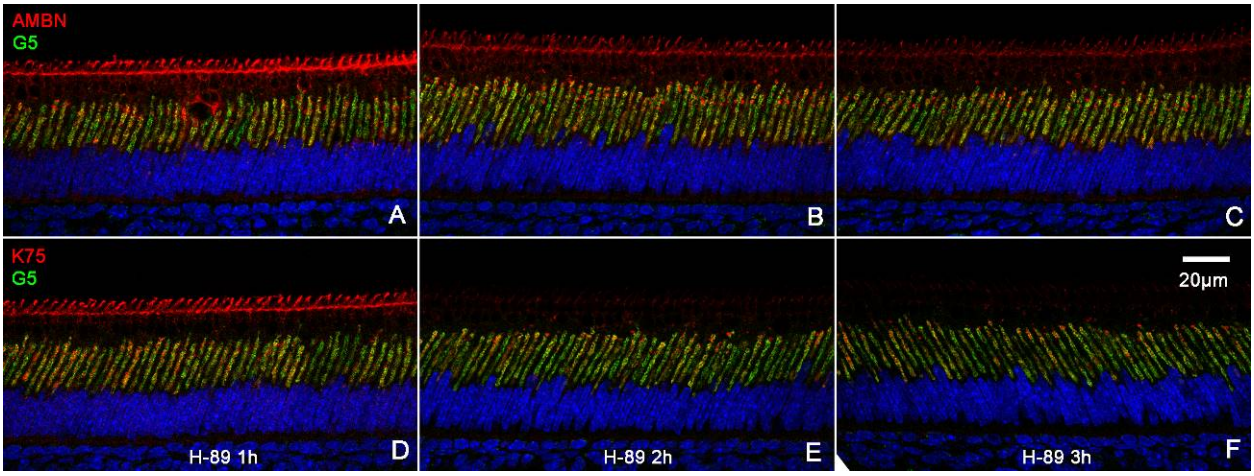

Figure 29. Effects of 0.5mg H-89 in ethanol on AMBN and K75 distribution, co-labelled with G5 after 1, 2 and 3 hours.

(A-C) Co-labelling of G5 and AMBN at 1, 2 and 3 hour points. (D-F) Co-labelling of G5 and K75 at 1, 2 and 3 hour points.

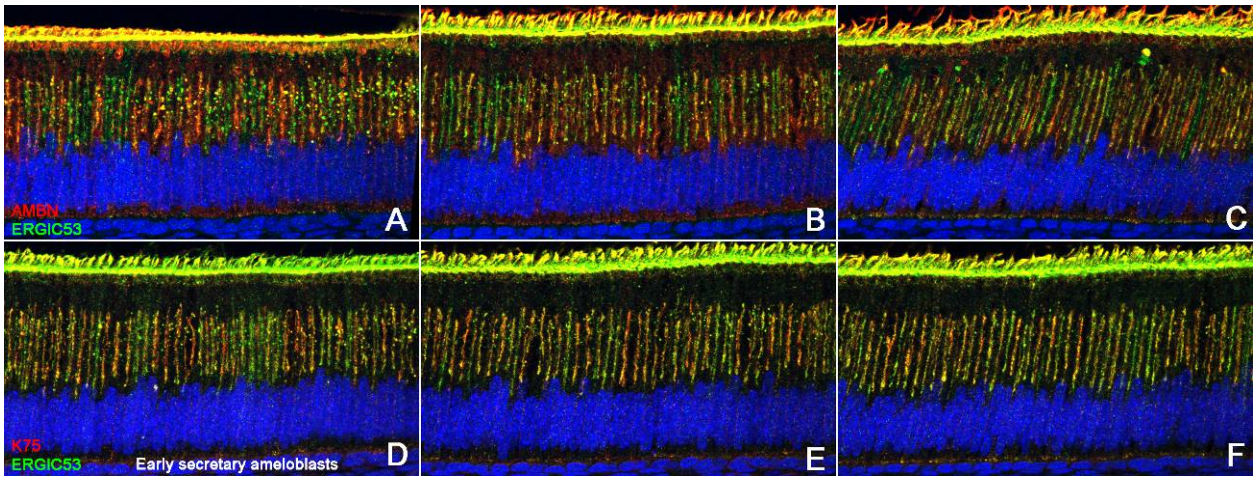

Figure 30. Early secretory stage ameloblasts showed more ERGIC granules compared with later ameloblasts.

(A-C) Co-labelling of AMBN and E53 in early secretory stage ameloblasts (A) and successively later period ameloblasts (B and C). (D-F) Co-labelling of K75 and E53 in early secretory stage ameloblasts (D) and successively later period ameloblasts (E and F).

5.0 DISCUSSION

In a recent study[37], K75 was found in mature enamel and ameloblasts. Although a number of papers suggested the presence of keratins in enamel, this was the first study in which it was clearly shown[24-26]. Moreover, a single amino acid substitution A161T in K75 was found to be highly associated with higher susceptibility to dental caries in human population. The present study further elaborated these earlier findings and provided detailed insights into the expression pattern of K75.

Our ISH studies of the craniofacial region of a mouse revealed a highly specific expression pattern of Krt75, with hair follicles, papillae of the tongue and developing teeth. While, Krt75 expression in hair follicles and papillae were previously described[28,29], the discovery of Krt75 expression in developing teeth is novel. Interestingly, in addition to expression of Krt75 in ameloblasts and stratum intermedium, the expression was also observed in odontoblasts. Keratins are typically associated with epithelium[27] and Krt75 expression in odontoblasts in unexpected, however considering that are ectomesenchymal cells of neural crest origin, it is not entirely impossible[83]. Western blot further confirmed the presence of K75 in forming pig enamel matrix.

Our mass spectroscopy studies of mature human insoluble enamel matrix identified a handful of sequences present in K75, however since these sequences are shared with other hair follicle keratins an unambiguous positive identification of K75 was impossible. However,

according to a personal communication of our collaborator, Dr. Yasuo Yamakoshi (Tsurumi University, Japan), it was possible to unequivocally identify K75 in secretory and maturation stage enamel matrix of unerupted pig molars by mass spectroscopy.

IF study of apical portions of constantly growing murine incisors revealed that K75 is expressed only during secretory stage of amelogenesis, at which the full thickness of enamel matrix is deposited. This is an important observation, as it suggests that K75 expression is associated with the enamel matrix deposition. K75 signal was also found in secretory enamel, and based on the signal pattern it was associated with enamel rod sheath and tufts, elements of the enamel matrix found in the mature enamel[23].

There is a big difference in the strength of the signal between the ISH and IF, i.e. low mRNA vs. high protein expression. It is especially interesting, since while stratum intermedium had a very strong ISH signal, the protein expression was quite modest in this cell layer. Furthermore, while mRNA expression was detected in odontoblasts no protein expression was observed in these cells. The difference between mRNA and protein expression levels was also observed in other systems. For example, a similar trend could be found for K2 in gastrointestinal tract (esophagus) tissue (Fig. 31), reversed correlations with high mRNA level and low protein level were also seen in many fields[84,85]. In fact, as there are many processes to regulate the transcription and translation, a correlation factor of only 40-60% was observed between mRNA and corresponding protein levels of expression[86,87]. Another important factor affecting protein quantities are the stability and degradation variances among all the proteins. For example, a very stable protein (like cytoskeleton proteins) with extremely limited turnover will exist longer and will not need high mRNA to be transcribed, while a rapidly degraded protein might need relatively high amount of mRNA to maintain its protein level.

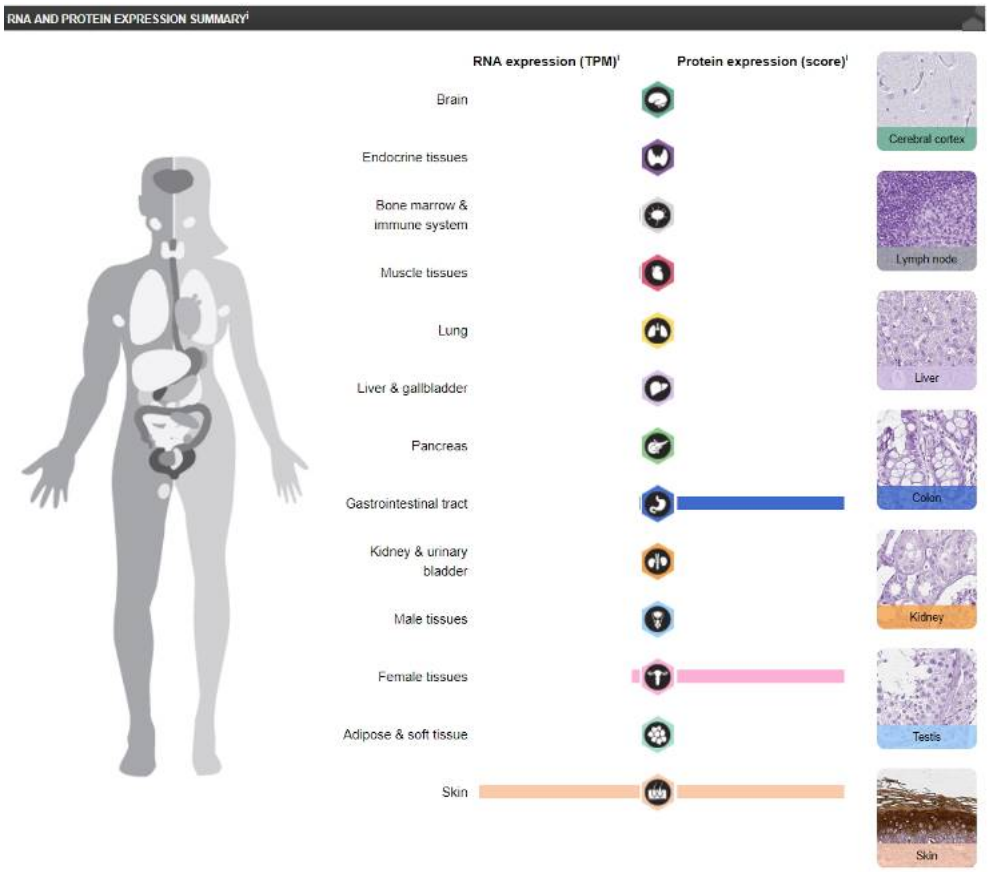

Figure 31. Expression of K2 in different human tissues.

Left side bars are RNA expression levels and the right side bars are corresponding protein expression levels. Be noted that in gastrointestinal tract and female tissues, the RNA and protein levels are un-matched. This information is cited from Human Protein Atlas at www.proteinatlas.org.

The IF distribution of K75 in secretory ameloblasts is dramatically different from that of typical cytokeratins, such as K5 or K14 which form dense networks of tonofilaments. In contrast K75 signal appears in two forms: large and small vesicles. Our IG-TEM revealed that K14 is strongly associated with tonofilaments (Fig. 32) while K75 is contained in membrane delineated vesicles of different sizes, which is highly unusual for a cytosolic protein, lacking a signal peptide. The presence of K75 containing vesicles in Tomes' processes and the surrounding matrix strongly suggested that it is secreted from ameloblasts. Remarkably, our double and triple

labeling IF and IG-TEM studies demonstrated a strong overlap of K75 with AMBN and AMELX (Fig. 8, 9). These observations strongly indicate that K75, despite the lack of the signal peptide, is at least partially involved in the conventional secretory pathway.

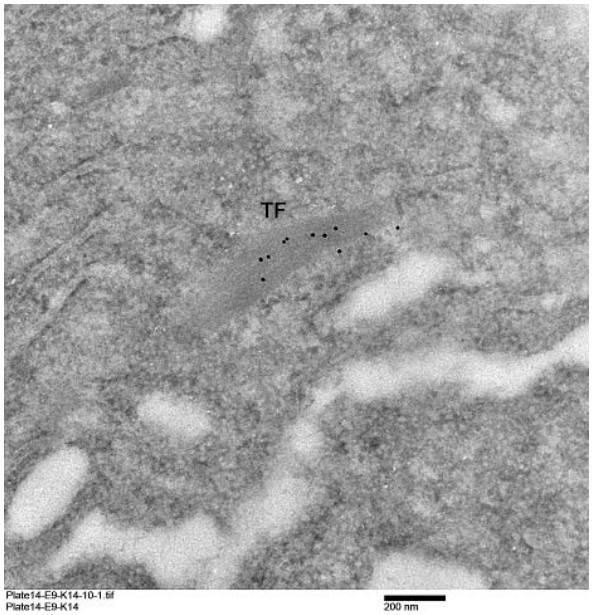

Figure 32. IG-TEM of a tonofilament (TF) in a rat secretory ameloblast labeled with antibodies against K14.

BFA is a fungi-derived toxin that has shown broad effects on membrane trafficking, e.g. Golgi tubulation with ER[72], trans-Golgi network (TGN) tubulation with early endosomes[88,89], disruption of microtubule and actin dynamics[90]. Meanwhile, its function seems to vary a lot when testing in different cell types, with different drug concentrations and duration time[91]. Pharmacological evidence suggests BFA as an uncompetitive inhibitor to retrograde COP1 vesicle formation by favoring the formation of a ARF-BFA-Sec7 complex[92,93]. Apparently, more investigations will be necessary to explain the complex effects of the drug. Nevertheless, BFA shows a very stable effect in most tested cell types, the inhibition of ER to Golgi trafficking. Our co-localization studies and BFA treatment experiments provide insights into the unconventional secretion of K75, a cytosolic protein lacking signal peptide, in ameloblasts. Unlike other

nonclassical secretory pathways of cytosolic proteins, which are independent from the rER-Golgi canonical secretory pathway[45], K75 is the first known cytosolic protein that utilizes part of the conventional ER-Golgi pathway. Specifically, it is present in secretory vesicles together with two major EMPs AMELX and AMBN, which possess the signal peptide and are secreted via classical secretory pathway[63,68]. K75 is also present in ERGIC and Golgi apparatus, cellular compartments associated with the classical secretory pathway, but not in the rER (Fig. 22,33,34). Furthermore, BFA treatment, which disrupts rER-Golgi transport (Fig. 35), did not significantly affect the presence of K75 in Golgi. Based on these results we propose a novel, unconventional secretory pathway for K75 (Fig. 34H). According to our model, K75 enters the classical secretory pathway not via rER, as the majority secreted proteins do, but it is translocated into the secretory system from the cytoplasm. Once in the ERGIC it is co-transported with other secretory cargo through the Golgi apparatus and secreted from the Tomes' processes. At the same time, the fact that the BFA treatment, which leads to dispersion of ERGIC (Fig. 36), does not significantly affect K75 co-localization with G5 suggests that another ERGIC independent mechanism of K75 translocation into the Golgi exists. To the best of our knowledge this is the first observation of a trafficking route for a cytosolic protein which utilizes portions of conventional rER-Golgi secretory pathway and it is very different from other unconventional pathways utilized by cytosolic proteins[45,94].

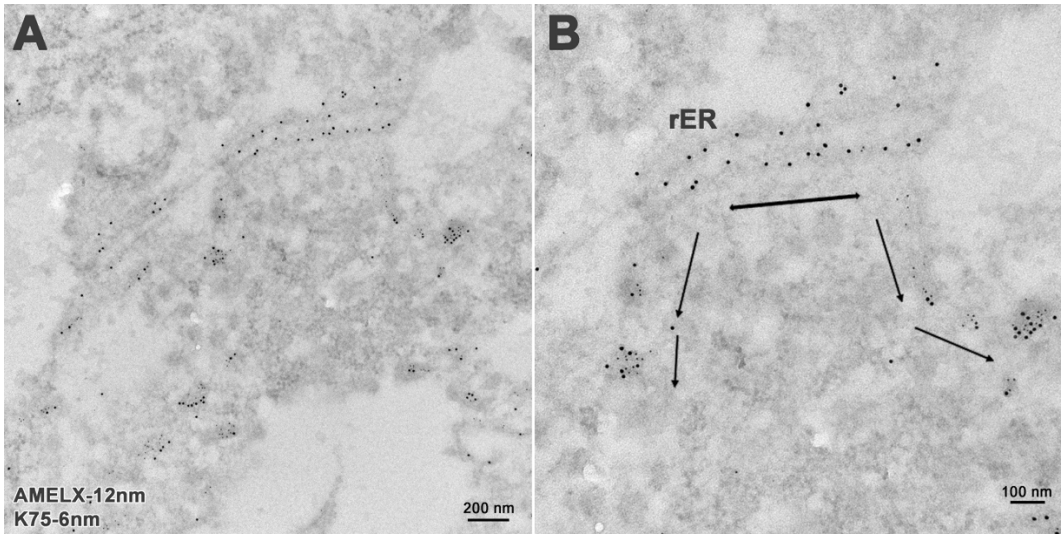

Figure 33. IG-TEM image showing AMELX and K75 are co-transported t together.

Note that abundance of AMELX translocate from what appears to be rER while K75 is not.

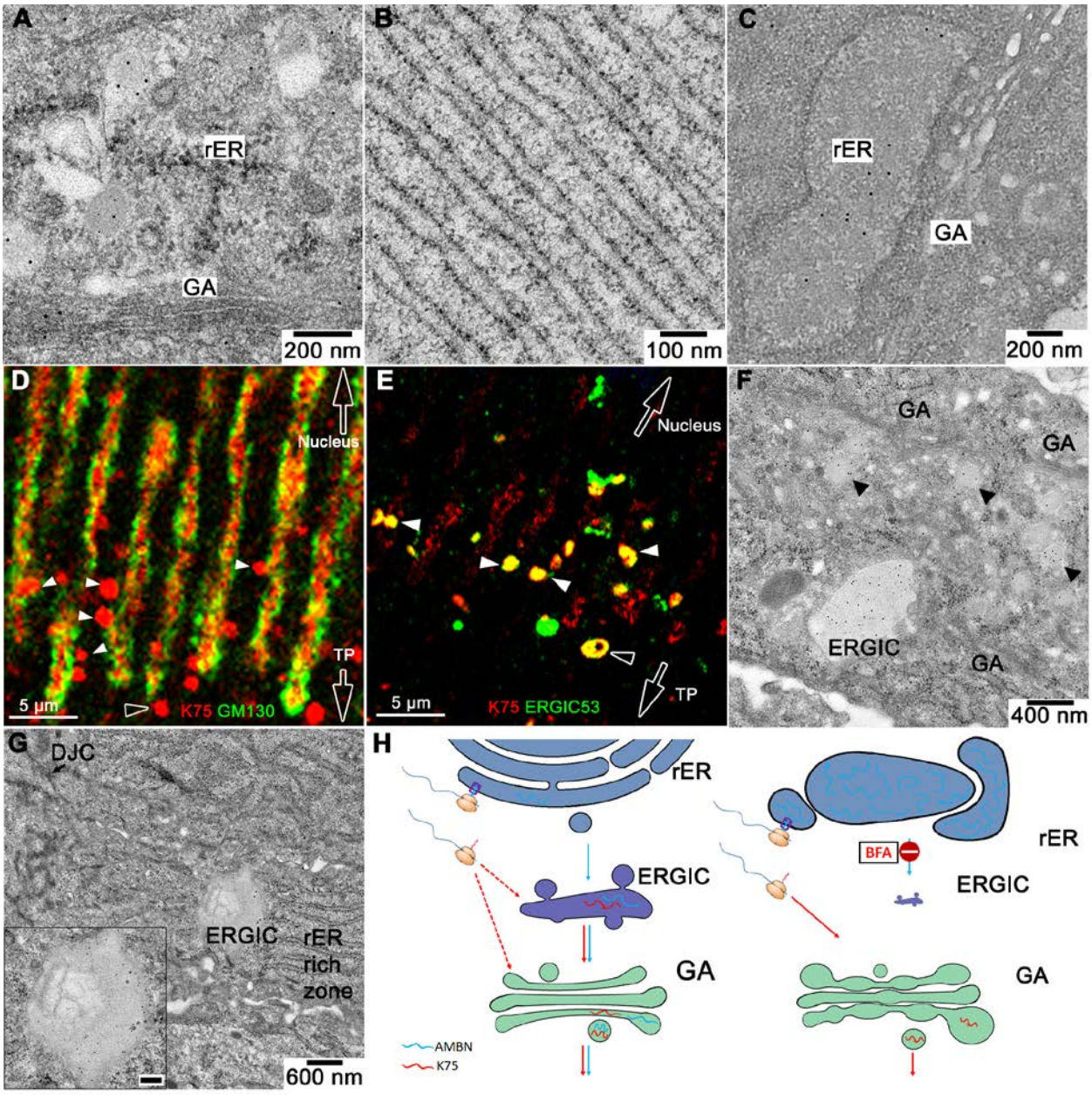

Figure 34. IG-TEM of mice ameloblasts after BFA treatment and schematic model for UPS of K75.

(A, B) IG-TEM for AMBN and K75 in vehicle controls. (C) AMBN was enriched in rER after BFA treatment. Note the dilated rER lumen, and the Golgi cisternae became widened, potentially due to the cessation of the retrograde transport, however, the overall organization of the Golgi apparatus remained unaffected. IF co-localization of K75 with GM130 and E53 (D, E) in the central portions of ameloblasts and IG-TEM micrographs (F, G) of the similar region. (D) High magnification IF image of co-localization of K75 and GM130 reveals two parallel strips of central Golgi complex and the K75 positive bands between them. Large K75 positive granules (white arrowheads) were

closely associated to the peripheral region of the Golgi strips and were present in the distal portions of ameloblasts (black arrowheads). (E) High magnification IF image of co-localization of K75 and E53. K75 overlapped with E53 in large granules in the central (white arrowheads) and distal (black arrowheads) portions of ameloblasts. (F) IG-TEM for K75 (6 nm) and AMBN (12 nm) of the central portion of ameloblast, revealed two strips of Golgi complex, outlining the cell core, filled with small secretory vesicles containing K75 and AMBN label (arrowheads). A large vesicle (presumably ERGIC) located at the periphery of the cell, was in a close proximity to the Golgi strip. Both types of vesicles contained label. (G) IG-TEM of the distal portion of the ameloblast. The area contains extensive rER and large granules, containing AMBN and K75 label, similar to those found in the central portion of ameloblast in F. K75, 6 nm gold particles; AMBN, 12 nm gold particles. Scale bars is 200 nm for inset. DJC – distal junctional complex; GA – Golgi apparatus; rER – rough endoplasmic reticulum; TP– Tomes' process. (H) Schematics of the proposed model for unconventional trafficking of K75 in ameloblasts, based on our IF co-localization studies and BFA treatment experiments. Under normal conditions K75 is synthesized in the cytoplasm and enters ERGIC, where it joints EMPs, i.e. AMBN, synthesized in the rER. The ERGIC cargo is transported to Golgi where it is packed into secretory vesicles and delivered to the secretory sites at the distal end of ameloblast. BFA treatment inhibits ER to Golgi transport, leading to accumulation of AMBN in the dilated rER lumen and depletion of AMBN in Golgi. At the same time, the BFA treatment does not affect translocation of K75 into Golgi, despite the fact that ERGIC is disrupted by BFA. This suggests that K75 utilizes an alternative ERGIC-independent trafficking pathway in addition to the ERGIC-Golgi route.

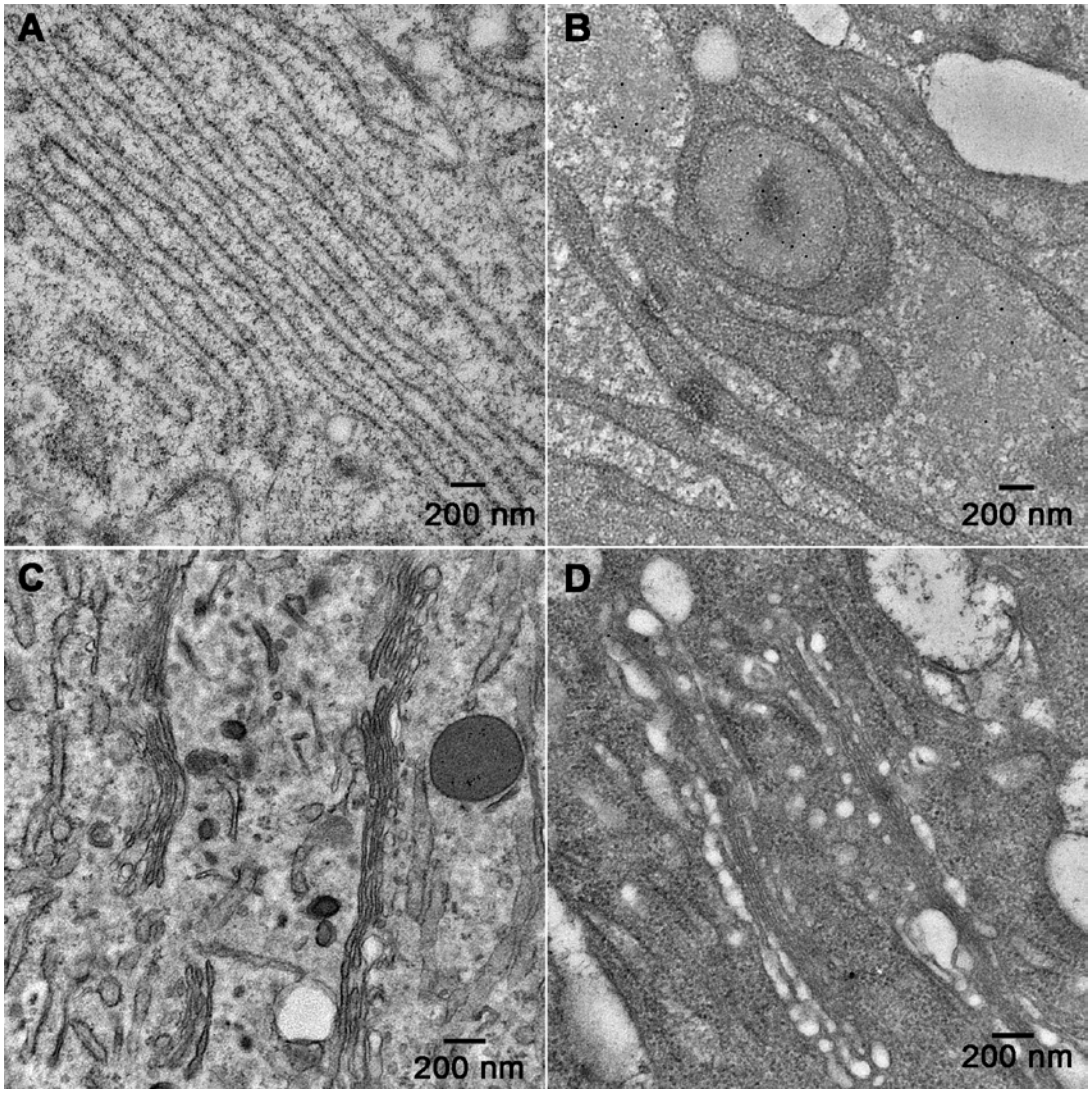

Figure 35. Comparison of ameloblast ultrastructure before and after BFA treatment.

(A, C) Ultrastructure of rER and Golgi before BFA treatment. (B, D) Ultrastructure of rER and Golgi after BFA treatment. Note the dilated ER lumen and vacuolization of Golgi cisternae.

Our observation of E53, in association with K75 and AMBN, in the distal rER rich zone of ameloblast and in the Tomes' processes raises the possibility that some elements of the ERGIC system can be involved in a secretory pathway that bypasses Golgi. One potential scenario is that some of these ERGIC structures are produced in the distal rER rich zone (34G) and transported into the Tomes' process directly. This hypothesis can provide a potential explanation to why there is a rER rich zone in the very distal end of ameloblast cell body.

Because it would be rather inexplicable if the proteins synthesized in distal rER zone are transported to the proximal Golgi complex and then travel back to the distal secretory apparatus. The presence of ERGIC signal in the distal ameloblast and Tomes' processes hints toward the possibility that another UPS mechanism, i.e. Golgi bypass by ERGIC coated vesicles exists in ameloblasts. It appears that, in ameloblasts, secreted proteins can simultaneously be transported via the conventional rER-Golgi pathway, as well as through the Golgi bypass mechanism[45,95,96] in E53-positive vesicles.

Another interesting question is the origin of LSCs. LSC could be several microns in diameter, while small secretory vesicles are 100-200 nm. There is no intermediate size of vesicles except the potential ERGIC, which could be over one micron in size. It is unclear whether LSC originates from small vesicles of Golgi or through ERGIC bypassing Golgi.

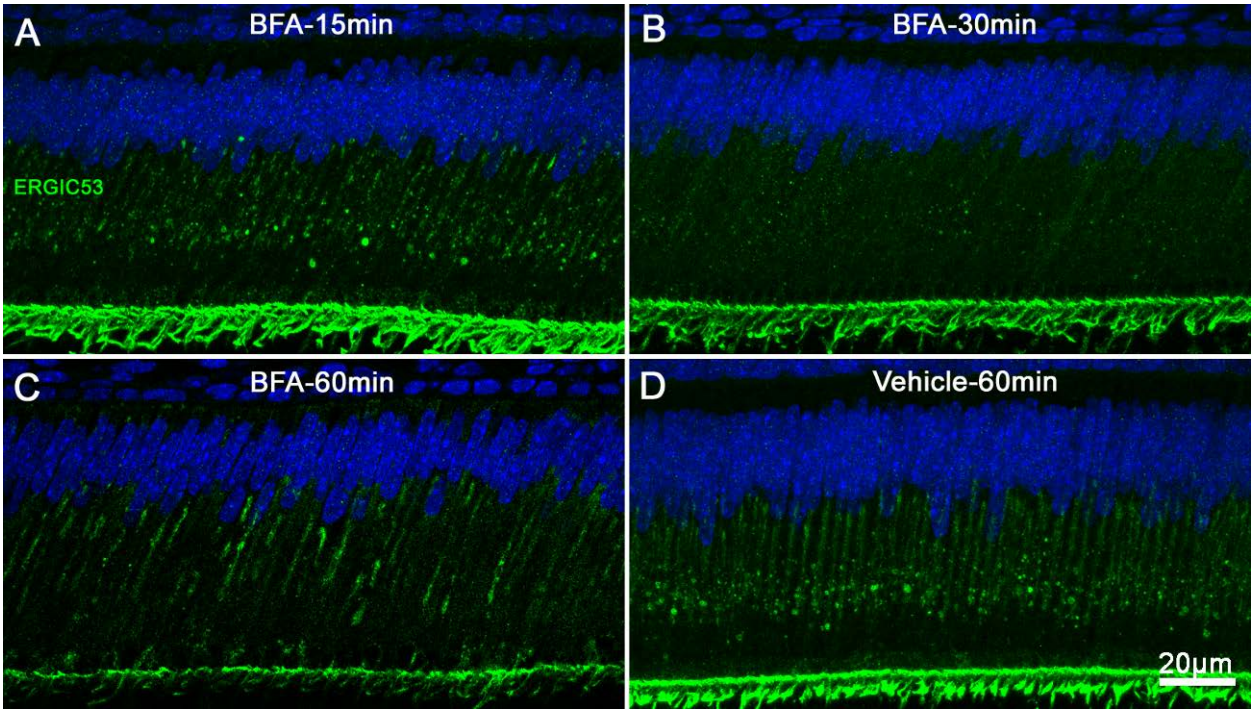

Figure 36. Changes in distribution of E53 signal in the BFA (PBS carrier) treated samples overtime.

(A) 15 min after injection the number of large ERGIC labeled granules was slightly less than in the vehicle control (D). (B) 30 min after the injection the ERGIC signal in the cytoplasm became dispersed, the large granules totally disappeared, (C) 60 min after the injection the ERGIC in cytoplasm started to recover, but ERGIC signal in the Tomes' processes were noticeably weaker than in the vehicle control or at the earlier time points.

Another issue regarding the trafficking in ameloblasts is concerned with the central Golgi complex. In general, evidence showed that *trans*-Golgi was facing the interior of ameloblast central Golgi complex and *cis*-Golgi was facing the cell membrane[13,14,97]. We also see a lot of secretory vesicles located in the internal space between the Golgi strips, indicating a major trafficking direction from outside to inside and from proximal to distal portions of ameloblasts. However, quite a few rER could also be seen inside the central Golgi complex (Fig. 11B,E,F). Considering the loose cylindric structure of Golgi complex and the existence of the intercellular accumulations[15], it is a reasonable to propose that there might be some reversed regions in the central Golgi complex which have their *trans* sides facing outward.

It is important to emphasize that ameloblasts are highly specialized super secretor cells and so far their secretory pathways can only be studied in vivo. In tissue cultures, ameloblast derived cells never attain their secretory phenotype. The vast majority of cell trafficking studies are conducted in tissue culture systems, and often the data obtained in vitro are not in agreement with in vivo observations, potentially because cells in vitro are not able to differentiate properly. We anticipate, that the mechanisms of secretions revealed in this study are not unique to ameloblasts but are much more universal and other cell types with high secretory activity might utilize them as well. Further in vivo studies conducted in other systems will be necessary to assess the relevance of this secretory pathway and to obtain better insights into the molecular mechanisms of this process.

Dental caries is the most prevalent chronic infectious disease in human population, with the prevalence of around 40% in children and around 90% in adults, according to data from NIH. Etiology of caries is complex and involves majorly four factors including microorganisms, oral environment, host susceptibility and time. While dental hygiene and healthy lifestyle would help to control microorganisms and improve oral environment, genetic factors determining caries susceptibility cannot be modified easily at the current state of science and technology. Earlier studies[37,82] revealed clear associations of certain polymorphisms in K75, K6, K16 and K17 with higher dental caries rate in human population. Knowing the genetic markers associated with the higher dental decay risks may lead to more individualized and effective preventions, especially when personalized or precision medicine era is approaching. Specifically, the carriers of these polymorphisms might require more aggressive prophylactics and more thorough monitoring and diagnostics. In addition to the caries prevention, understanding the basic biology of keratins in enamel formation, and their functional roles in mature enamel will inform the future design of novel restorative materials.

6.0 CONCLUSION

In conclusion, our studies provide a strong support to the previous observations of K75 in ameloblasts and enamel based on the evidence from ISH, IF, IG-TEM and Mass spectrometry studies. We determined that the expression of this protein is restricted in secretory stage ameloblasts. Furthermore, we found that K75 is co-transported together with other EMPs and is secreted from the Tomes' processes. We further established that under physiological conditions, K75 is present in ERGIC, central Golgi complex and secretory vesicles of the cell body and Tomes' processes but not in rER, using IF co-localization *in vivo* experiments, using cell compartment markers. These results suggest that K75 might enter the classic secretory pathway via ERGIC. BFA trafficking inhibition in mice further suggest that K75 could directly translocate in Golgi, bypassing both rER and ERGIC. Importantly, our results for the first time show cytosolic protein can utilize portions of the classical ER-ERGIC secretory pathway. However, the mechanism of this novel UPS pathway is currently unknown. Nevertheless it is clear that this mechanism is radically different from the previously reported UPS of cytosolic proteins[45,46]. Taken together, our results provide novel insights into the K75 secretion processes and raise questions regarding basic cellular trafficking mechanisms in ameloblasts and potentially other systems. This study also highlights potential novel roles of keratins, beyond cytoskeleton.

BIBLIOGRAPHY

1 Hu, J. C. C., Chun, Y. H. P., Al Hazzazzi, T. & Simmer, J. P. Enamel Formation and Amelogenesis Imperfecta. *Cells Tissues Organs* **186**, 78-85 (2007).

2 Garant, P. R. & Nalbandian, J. Observations on the ultrastructure of ameloblasts with special reference to the Golgi complex and related components. *J. Ultrastruct. Res.* **23**, 427-443, doi:http://dx.doi.org/10.1016/S0022-5320(68)80108-X (1968).

3 Katchburian, E. & Holt, S. J. Studies on the Development of Ameloblasts. *J. Cell Sci.* **11**, 415-447 (1972).

4 Warshawsky, H. The fine structure of secretory ameloblasts in rat incisors. *The Anatomical record* **161**, 211-229, doi:10.1002/ar.1091610207 (1968).

5 Bajaj, D. & Arola, D. D. On the R-curve behavior of human tooth enamel. *Biomaterials* **30**, 4037-4046, doi:10.1016/j.biomaterials.2009.04.017 (2009).

6 Baldassarri, M., Margolis, H. C. & Beniash, E. Compositional determinants of mechanical properties of enamel. *J. Dent. Res.* **87**, 645-649 (2008).

7 Chai, H., Lee, J. J. W., Constantino, P. J., Lucas, P. W. & Lawn, B. R. Remarkable resilience of teeth. *Proc Natl Acad Sci U S A* **106**, 7289-7293 (2009).

8 Macho, G. A., Jiang, Y. & Spears, I. R. Enamel micro structure - a truly three-dimensional structure. *J. Hum. Evol.* **45**, 81-90, doi:10.1016/s0047-2484(03)00083-6 (2003).

9 Travis, D. F. & Glimcher, M. J. The structure and organization of, and the relationship between the organic matrix and the inorganic crystals of embryonic bovine enamel. *J. Cell Biol.* **23**, 447-497, doi:10.1083/jcb.23.3.447 (1964).

10 Robinson, C. & Hudson, J. Tuft protein: protein cross-linking in enamel development. *Eur. J. Oral Sci.* **119 Suppl 1**, 50-54, doi:10.1111/j.1600-0722.2011.00906.x (2011).

11 Robinson, C., Fuchs, P. & Weatherell, J. A. Fate of matrix proteins during development of dental enamel. *Calcif. Tissue Res.* **22**, 185-190 (1977).

12 Sasaki, T. Ultrastructure and cytochemistry of the Golgi apparatus and related organelles of the secretory ameloblasts of the rat incisor. *Arch Oral Biol* **28**, 895-905, doi:http://dx.doi.org/10.1016/0003-9969(83)90084-5 (1983).

13 Smith, C. E. Ultrastructural localization of nicotinamide adenine dinucleotide phosphatase (NADPase) activity to the intermediate saccules of the Golgi apparatus in rat incisor ameloblasts. *J Histochem Cytochem* **28**, 16-26, doi:10.1177/28.1.7351472 (1980).

14 Smith, C. E. Ultrastructural localization of coenzyme A phosphatase (CoA-Pase) activity to the GERL system in secretory ameloblasts of the rat incisor. *J Histochem Cytochem* **29**, 1243-1254, doi:10.1177/29.11.6172461 (1981).

15 Smith, C. E., Hu, Y., Hu, J. C. C. & Simmer, J. P. Ultrastructure of early amelogenesis in wild-type, Amelx-/-, and Enam-/- mice: enamel ribbon initiation on dentin mineral and

ribbon orientation by ameloblasts. *Molecular Genetics & Genomic Medicine* **4**, 662-683, doi:10.1002/mgg3.253 (2016).
16 Bartlett, J. D. Dental Enamel Development: Proteinases and Their Enamel Matrix Substrates. *ISRN Dentistry* **2013**, 684607, doi:10.1155/2013/684607 (2013).
17 Glimcher, M. J. & Levine, P. T. Studies of the proteins, peptides and free amino acids of mature bovine enamel. *Biochem J* **98**, 742-753 (1966).
18 Weidmann, S. M. & Eyre, D. R. in *International Symposium on Tooth Enamel* (eds M.V. Stack & R.W. Fearnhead) (John Wright & Sons, 1971).
19 Robinson, C., Lowe, N. R. & Weatherell, J. A. Changes in amino-acid composition of developing rat incisor enamel. *Calcif. Tissue Res.* **23**, 19-31 (1977).
20 Belcourt, A. Normal Mature Human Enamel Protein. *J. Dent. Res.* **58**, 986-987, doi:10.1177/00220345790580025301 (1979).
21 Belcourt, A. & Gillmeth, S. EDTA soluble protein of human mature normal enamel. *Calcif. Tissue Int.* **28**, 227-231, doi:10.1007/BF02441240 (1979).
22 Osborn, J. W. The 3-dimensional morphology of the tufts in human enamel. *Acta Anat. (Basel)* **73**, 481-495 (1969).
23 Amizuka, N., Uchida, T., Fukae, M., Yamada, M. & Ozawa, H. Ultrastructural and Immunocytochemical Studies of Enamel Tufts in Human Permanent Teeth. *Arch. Histol. Cytol.* **55**, 179-190, doi:10.1679/aohc.55.179 (1992).
24 Robinson, C., Shore, R. C. & Kirkham, J. Tuft protein: its relationship with the keratins and the developing enamel matrix. *Calcif Tissue Int* **44**, 393-398 (1989).
25 Pautard, F. G. MINERALIZATION OF KERATIN AND ITS COMPARISON WITH THE ENAMEL MATRIX. *Nature* **199**, 531-535 (1963).
26 Duverger, O., Beniash, E. & Morasso, M. I. Keratins as components of the enamel organic matrix. *Matrix Biol.* **52-54**, 260-265, doi:10.1016/j.matbio.2015.12.007 (2016).
27 Moll, R., Divo, M. & Langbein, L. The human keratins: biology and pathology. *Histochem Cell Biol* **129**, 705-733, doi:10.1007/s00418-008-0435-6 (2008).
28 Winter, H. *et al.* A Novel Human Type II Cytokeratin, K6hf, Specifically Expressed in the Companion Layer of the Hair Follicle. *J. Invest. Dermatol.* **111**, 955-962, doi:https://doi.org/10.1046/j.1523-1747.1998.00456.x (1998).
29 Wang, Z., Wong, P., Langbein, L., Schweizer, J. & Coulombe, P. A. Type II Epithelial Keratin 6hf (K6hf) Is Expressed in the Companion Layer, Matrix, and Medulla in Anagen-Stage Hair Follicles. *J. Invest. Dermatol.* **121**, 1276-1282, doi:http://dx.doi.org/10.1111/j.1523-1747.2003.12644.x (2003).
30 Sperling, L. C., Hussey, S., Sorrells, T., Wang, J. A. & Darling, T. Cytokeratin 75 expression in central, centrifugal, cicatricial alopecia--new observations in normal and diseased hair follicles. *J. Cutan. Pathol.* **37**, 243-248, doi:10.1111/j.1600-0560.2009.01330.x (2010).
31 Wojcik, S. M., Longley, M. A. & Roop, D. R. Discovery of a novel murine keratin 6 (K6) isoform explains the absence of hair and nail defects in mice deficient for K6a and K6b. *J Cell Biol* **154**, 619-630, doi:10.1083/jcb.200102079 (2001).
32 Chen, J. *et al.* Mice expressing a mutant Krt75 (K6hf) allele develop hair and nail defects resembling pachyonychia congenita. *J. Invest. Dermatol.* **128**, 270-279, doi:10.1038/sj.jid.5701038 (2008).
33 Lin, S. J. *et al.* Feather regeneration as a model for organogenesis. *Dev Growth Differ* **55**, 139-148, doi:10.1111/dgd.12024 (2013).

34 Winter, H. *et al.* An unusual Ala12Thr polymorphism in the 1A alpha-helical segment of the companion layer-specific keratin K6hf: evidence for a risk factor in the etiology of the common hair disorder pseudofolliculitis barbae. *J. Invest. Dermatol.* **122**, 652-657, doi:10.1111/j.0022-202X.2004.22309.x (2004).
35 McLean, W. H. Close shave for a keratin disorder-K6hf polymorphism linked to Pseudofolliculitis barbae. *J. Invest. Dermatol.* **122**, xi-xiii, doi:10.1111/j.0022-202X.2004.22351.x (2004).
36 Jasterzbski, T. J. & Schwartz, R. A. Pseudofolliculitis cutis: a vexing disorder of hair growth. *Br. J. Dermatol.* **172**, 878-884, doi:10.1111/bjd.13427 (2015).
37 Duverger, O. *et al.* Hair keratin mutations in tooth enamel increase dental decay risk. *J. Clin. Invest.* **124**, 5219-5224, doi:10.1172/JCI78272 (2014).
38 Rothman, J. E. Mechanisms of intracellular protein transport. *Nature* **372**, 55-63, doi:10.1038/372055a0 (1994).
39 Lee, M. C., Miller, E. A., Goldberg, J., Orci, L. & Schekman, R. Bi-directional protein transport between the ER and Golgi. *Annu Rev Cell Dev Biol* **20**, 87-123, doi:10.1146/annurev.cellbio.20.010403.105307 (2004).
40 Schuldiner, M. *et al.* The GET Complex Mediates Insertion of Tail-Anchored Proteins into the ER Membrane. *Cell* **134**, 634-645, doi:https://doi.org/10.1016/j.cell.2008.06.025 (2008).
41 Bonifacino, J. S. & Glick, B. S. The mechanisms of vesicle budding and fusion. *Cell* **116**, 153-166 (2004).
42 Gurkan, C., Stagg, S. M., Lapointe, P. & Balch, W. E. The COPII cage: unifying principles of vesicle coat assembly. *Nature reviews. Molecular cell biology* **7**, 727-738, doi:10.1038/nrm2025 (2006).
43 Stagg, S. M. *et al.* Structural basis for cargo regulation of COPII coat assembly. *Cell* **134**, 474-484, doi:10.1016/j.cell.2008.06.024 (2008).
44 Mellman, I. & Warren, G. The road taken: past and future foundations of membrane traffic. *Cell* **100**, 99-112 (2000).
45 Nickel, W. & Rabouille, C. Mechanisms of regulated unconventional protein secretion. *Nat. Rev. Mol. Cell Biol.* **10**, 148-155, doi:10.1038/nrm2617 (2009).
46 Rabouille, C. Pathways of Unconventional Protein Secretion. *Trends Cell Biol* **27**, 230-240, doi:10.1016/j.tcb.2016.11.007 (2017).
47 Steringer, J. P., Müller, H.-M. & Nickel, W. Unconventional Secretion of Fibroblast Growth Factor 2—A Novel Type of Protein Translocation across Membranes? *Journal of Molecular Biology* **427**, 1202-1210, doi:http://dx.doi.org/10.1016/j.jmb.2014.07.012 (2015).
48 La Venuta, G., Zeitler, M., Steringer, J. P., Müller, H.-M. & Nickel, W. The Startling Properties of Fibroblast Growth Factor 2: How to Exit Mammalian Cells without a Signal Peptide at Hand. *Journal of Biological Chemistry* **290**, 27015-27020, doi:10.1074/jbc.R115.689257 (2015).
49 Debaisieux, S., Rayne, F., Yezid, H. & Beaumelle, B. The Ins and Outs of HIV-1 Tat. *Traffic* **13**, 355-363, doi:10.1111/j.1600-0854.2011.01286.x (2012).
50 Steringer, J. P. *et al.* Phosphatidylinositol 4,5-Bisphosphate (PI(4,5)P2)-dependent Oligomerization of Fibroblast Growth Factor 2 (FGF2) Triggers the Formation of a Lipidic Membrane Pore Implicated in Unconventional Secretion. *Journal of Biological Chemistry* **287**, 27659-27669, doi:10.1074/jbc.M112.381939 (2012).

51 Pamer, E. & Cresswell, P. MECHANISMS OF MHC CLASS I–RESTRICTED ANTIGEN PROCESSING. *Annual Review of Immunology* **16**, 323-358, doi:10.1146/annurev.immunol.16.1.323 (1998).
52 Borst, P., Zelcer, N. & van Helvoort, A. ABC transporters in lipid transport. *Biochimica et Biophysica Acta (BBA) - Molecular and Cell Biology of Lipids* **1486**, 128-144, doi:https://doi.org/10.1016/S1388-1981(00)00053-6 (2000).
53 Andrei, C. *et al.* The Secretory Route of the Leaderless Protein Interleukin 1β Involves Exocytosis of Endolysosome-related Vesicles. *Molecular Biology of the Cell* **10**, 1463-1475, doi:10.1091/mbc.10.5.1463 (1999).
54 Andrei, C. *et al.* Phospholipases C and A2 control lysosome-mediated IL-1β secretion: Implications for inflammatory processes. *Proceedings of the National Academy of Sciences of the United States of America* **101**, 9745-9750, doi:10.1073/pnas.0308558101 (2004).
55 Fatal, N., Karhinen, L., Jokitalo, E. & Makarow, M. Active and specific recruitment of a soluble cargo protein for endoplasmic reticulum exit in the absence of functional COPII component Sec24p. *Journal of Cell Science* **117**, 1665-1673, doi:10.1242/jcs.01019 (2004).
56 Gee, Heon Y., Noh, Shin H., Tang, Bor L., Kim, Kyung H. & Lee, Min G. • Rescue of △F508-CFTR Trafficking via a GRASP-Dependent Unconventional Secretion Pathway. *Cell* **146**, 746-760, doi:10.1016/j.cell.2011.07.021 (2011).
57 Hardwick, K. G. & Pelham, H. R. SED5 encodes a 39-kD integral membrane protein required for vesicular transport between the ER and the Golgi complex. *The Journal of cell biology* **119**, 513-521, doi:10.1083/jcb.119.3.513 (1992).
58 Amessou, M. *et al.* Syntaxin 16 and syntaxin 5 are required for efficient retrograde transport of several exogenous and endogenous cargo proteins. *Journal of Cell Science* **120**, 1457-1468, doi:10.1242/jcs.03436 (2007).
59 Schotman, H., Karhinen, L. & Rabouille, C. dGRASP-Mediated Noncanonical Integrin Secretion Is Required for Drosophila Epithelial Remodeling. *Developmental Cell* **14**, 171-182, doi:http://dx.doi.org/10.1016/j.devcel.2007.12.006 (2008).
60 Dupont, N. *et al.* Autophagy‐based unconventional secretory pathway for extracellular delivery of IL‐1β. *The EMBO Journal* **30**, 4701-4711, doi:10.1038/emboj.2011.398 (2011).
61 Baldwin, T. A. & Ostergaard, H. L. The Protein-tyrosine Phosphatase CD45 Reaches the Cell Surface via Golgi-dependent and -independent Pathways. *Journal of Biological Chemistry* **277**, 50333-50340, doi:10.1074/jbc.M209075200 (2002).
62 Della Valle, M. C. *et al.* Classification of Subcellular Location by Comparative Proteomic Analysis of Native and Density-shifted Lysosomes. *Molecular & Cellular Proteomics* **10**, doi:10.1074/mcp.M110.006403 (2011).
63 Zalzal, S. F., Smith, C. E. & Nanci, A. Ameloblastin and amelogenin share a common secretory pathway and are co-secreted during enamel formation. *Matrix Biol.* **27**, 352-359, doi:10.1016/j.matbio.2008.01.003 (2008).
64 Verdelis, K. *et al.* Accelerated enamel mineralization in Dspp mutant mice. *Matrix Biol.* **52-54**, 246-259, doi:10.1016/j.matbio.2016.01.003 (2016).
65 Szabo-Rogers, H. L. *et al.* Novel skeletogenic patterning roles for the olfactory pit. *Development* **136**, 219-229, doi:10.1242/dev.023978 (2009).

66 Yang, X., Vidunas, A. & Beniash, E. Optimizing Immunostaining of Enamel Matrix: Application of Sudan Black B and Minimization of False Positives from Normal Sera and IgGs. *Front. Physiol.* **8**, doi:10.3389/fphys.2017.00239 (2017).
67 Rice, R. H. *et al.* Differentiating Inbred Mouse Strains from Each Other and Those with Single Gene Mutations Using Hair Proteomics. *PLOS ONE* **7**, e51956, doi:10.1371/journal.pone.0051956 (2012).
68 Nanci, A. *et al.* Comparative immunochemical analyses of the developmental expression and distribution of ameloblastin and amelogenin in rat incisors. *J. Histochem. Cytochem.* **46**, 911-934 (1998).
69 Begue-Kirn, C., Krebsbach, P. H., Bartlett, J. D. & Butler, W. T. Dentin sialoprotein, dentin phosphoprotein, enamelysin and ameloblastin: tooth-specific molecules that are distinctively expressed during murine dental differentiation. *Eur. J. Oral Sci.* **106**, 963-970, doi:10.1046/j.0909-8836.1998.eos106510.x (1998).
70 Bleicher, F., Couble, M. L., Farges, J. C., Couble, P. & Magloire, H. Sequential expression of matrix protein genes in developing rat teeth. *Matrix Biol.* **18**, 133-143, doi:10.1016/s0945-053x(99)00007-4 (1999).
71 Gregory, K. E. *et al.* Structural Organization of Distinct Domains within the Non-collagenous N-terminal Region of Collagen Type XI. *J. Biol. Chem.* **275**, 11498-11506, doi:10.1074/jbc.275.15.11498 (2000).
72 Lippincott-Schwartz, J., Yuan, L. C., Bonifacino, J. S. & Klausner, R. D. Rapid redistribution of Golgi proteins into the ER in cells treated with brefeldin A: Evidence for membrane cycling from Golgi to ER. *Cell* **56**, 801-813, doi:10.1016/0092-8674(89)90685-5 (1989).
73 Nanci, A. *et al.* Comparative Immunochemical Analyses of the Developmental Expression and Distribution of Ameloblastin and Amelogenin in Rat Incisors. *J. Histochem. Cytochem.* **46**, 911-934, doi:10.1177/002215549804600806 (1998).
74 Nickel, W. The mystery of nonclassical protein secretion. *Eur. J. Biochem.* **270**, 2109-2119, doi:10.1046/j.1432-1033.2003.03577.x (2003).
75 Lochner, A. & Moolman, J. A. The Many Faces of H89: A Review. *Cardiovasc. Drug Rev.* **24**, 261-274, doi:10.1111/j.1527-3466.2006.00261.x (2006).
76 Muñiz, M., Alonso, M., Hidalgo, J. & Velasco, A. A Regulatory Role for cAMP-dependent Protein Kinase in Protein Traffic along the Exocytic Route. *J. Biol. Chem.* **271**, 30935-30941, doi:10.1074/jbc.271.48.30935 (1996).
77 Muñiz, M., Martín, M. E., Hidalgo, J. & Velasco, A. Protein kinase A activity is required for the budding of constitutive transport vesicles from the trans-Golgi network. *Proceedings of the National Academy of Sciences* **94**, 14461-14466 (1997).
78 Jamora, C. *et al.* Gβγ-Mediated Regulation of Golgi Organization Is through the Direct Activation of Protein Kinase D. *Cell* **98**, 59-68, doi:http://dx.doi.org/10.1016/S0092-8674(00)80606-6 (1999).
79 Lee, T. H. & Linstedt, A. D. Potential Role for Protein Kinases in Regulation of Bidirectional Endoplasmic Reticulum-to-Golgi Transport Revealed by Protein Kinase Inhibitor H89. *Mol Biol Cell* **11**, 2577-2590 (2000).
80 Aridor, M. & Balch, W. E. Kinase Signaling Initiates Coat Complex II (COPII) Recruitment and Export from the Mammalian Endoplasmic Reticulum. *J. Biol. Chem.* **275**, 35673-35676, doi:10.1074/jbc.C000449200 (2000).

81 Bejarano, E., Cabrera, M., Vega, L., Hidalgo, J. & Velasco, A. Golgi structural stability and biogenesis depend on associated PKA activity. *J. Cell Sci.* **119**, 3764 (2006).
82 Duverger, O. *et al.* Genetic variants in pachyonychia congenita-associated keratins increase susceptibility to tooth decay. *PLoS Genet* **14**, e1007168, doi:10.1371/journal.pgen.1007168 (2018).
83 Katagata, Y., Aoki, T., Kawa, Y., Mizoguchi, M. & Kondo, S. Keratin subunit expression in human cultured melanocytes and mouse neural crest cells without formation of filamentous structures. *J. Investig. Dermatol. Symp. Proc.* **4**, 110-115 (1999).
84 Meierhofer, D. *et al.* Protein sets define disease states and predict in vivo effects of drug treatment. *Mol. Cell. Proteomics* **12**, 1965-1979, doi:10.1074/mcp.M112.025031 (2013).
85 Anderson, L. & Seilhamer, J. A comparison of selected mRNA and protein abundances in human liver. *Electrophoresis* **18**, 533-537, doi:10.1002/elps.1150180333 (1997).
86 Tian, Q. *et al.* Integrated genomic and proteomic analyses of gene expression in Mammalian cells. *Mol. Cell. Proteomics* **3**, 960-969, doi:10.1074/mcp.M400055-MCP200 (2004).
87 Vogel, C. & Marcotte, E. M. Insights into the regulation of protein abundance from proteomic and transcriptomic analyses. *Nat Rev Genet* **13**, 227-232, doi:10.1038/nrg3185 (2012).
88 Lippincott-Schwartz, J. *et al.* Brefeldin A's effects on endosomes, lysosomes, and the TGN suggest a general mechanism for regulating organelle structure and membrane traffic. *Cell* **67**, 601-616, doi:http://dx.doi.org/10.1016/0092-8674(91)90534-6 (1991).
89 Wood, S. A., Park, J. E. & Brown, W. J. Brefeldin A causes a microtubule-mediated fusion of the trans-Golgi network and early endosomes. *Cell* **67**, 591-600, doi:http://dx.doi.org/10.1016/0092-8674(91)90533-5 (1991).
90 Alvarez, C. & Sztul, E. S. Brefeldin A (BFA) disrupts the organization of the microtubule and the actin cytoskeletons. *European Journal of Cell Biology* **78**, 1-14, doi:http://dx.doi.org/10.1016/S0171-9335(99)80002-8 (1999).
91 Grieve, A. G. & Rabouille, C. Golgi Bypass: Skirting Around the Heart of Classical Secretion. *Cold Spring Harbor Perspectives in Biology* **3**, a005298, doi:10.1101/cshperspect.a005298 (2011).
92 Chardin, P. & McCormick, F. Brefeldin A. *Cell* **97**, 153-155, doi:10.1016/S0092-8674(00)80724-2.
93 Peyroche, A. *et al.* Brefeldin A acts to stabilize an abortive ARF-GDP-Sec7 domain protein complex: involvement of specific residues of the Sec7 domain. *Molecular cell* **3**, 275-285 (1999).
94 Rabouille, C., Malhotra, V. & Nickel, W. Diversity in unconventional protein secretion. *J. Cell Sci.* **125**, 5251 (2013).
95 Grieve, A. G. & Rabouille, C. Golgi Bypass: Skirting Around the Heart of Classical Secretion. *Cold Spring Harb. Perspect. Biol.* **3**, doi:10.1101/cshperspect.a005298 (2011).
96 Rabouille, C. Pathways of Unconventional Protein Secretion. *Trends Cell Biol.* **27**, 230-240, doi:10.1016/j.tcb.2016.11.007 (2017).
97 Matsuo, S., Ichikawa, H., Wakisaka, S. & Akai, M. Changes of cytochemical properties in the Golgi apparatus during in vivo differentiation of the ameloblast in developing rat molar tooth germs. *Anat Rec* **234**, 469-478, doi:10.1002/ar.1092340403 (1992).